University of Zurich[UZH]

Zurich Open Repository and Archive
University of Zurich
Main Library
Strickhofstrasse 39
CH-8057 Zurich
www.zora.uzh.ch

Year: 2021

Absence of MMACHC in peripheral retinal cells does not lead to an ocular phenotype in mice

Kiessling, Eva ; Nötzli, Sarah ; Todorova, Vyara ; Forny, Merima ; Baumgartner, Matthias R ; Samardzija, Marijana ; Krijt, Jakub ; Kožich, Viktor ; Grimm, Christian ; Froese, D Sean

Abstract: Combined methylmalonic aciduria with homocystinuria (cblC type) is a rare disease caused by mutations in the MMACHC gene. MMACHC encodes an enzyme crucial for intracellular vitamin B_{12} metabolism, leading to the accumulation of toxic metabolites e.g. methylmalonic acid (MMA) and homocysteine (Hcy), and secondary disturbances in folate and one-carbon metabolism when not fully functional. Patients with cblC deficiency often present in the neonatal or early childhood period with a severe multisystem pathology, which comprises a broad spectrum of treatment-resistant ophthalmological phenotypes, including retinal degeneration, impaired vision, and vascular changes. To examine the potential function of MMACHC in the retina and how its loss may impact disease, we performed gene expression studies in human and mouse, which showed that local expression of MMACHC in the retina and retinal pigment epithelium is relatively stable over time. To study whether functional MMACHC is required for retinal function and tissue integrity, we generated a transgenic mouse lacking Mmachc expression in cells of the peripheral retina. Characterization of this mouse revealed accumulation of cblC disease related metabolites, including MMA and the folate-dependent purine synthesis intermediates AICA-riboside and SAICA-riboside in the retina. Nevertheless, fundus appearance, morphology, vasculature, and cellular composition of the retina, as well as ocular function, remained normal in mice up to 6 or 12 months of age. Our data indicates that peripheral retinal neurons do not require intrinsic expression of Mmachc for survival and function and questions whether a local MMACHC deficiency is responsible for the retinal phenotypes in patients.

DOI: https://doi.org/10.1016/j.bbadis.2021.166201

Posted at the Zurich Open Repository and Archive, University of Zurich
ZORA URL: https://doi.org/10.5167/uzh-208682
Journal Article
Published Version

The following work is licensed under a Creative Commons: Attribution 4.0 International (CC BY 4.0) License.

Originally published at:
Kiessling, Eva; Nötzli, Sarah; Todorova, Vyara; Forny, Merima; Baumgartner, Matthias R; Samardzija, Marijana; Krijt, Jakub; Kožich, Viktor; Grimm, Christian; Froese, D Sean (2021). Absence of MMACHC

in peripheral retinal cells does not lead to an ocular phenotype in mice. Biochimica et Biophysica Acta. Molecular Basis of Disease, 1867(10):166201.
DOI: https://doi.org/10.1016/j.bbadis.2021.166201

BBA - Molecular Basis of Disease 1867 (2021) 166201

Contents lists available at ScienceDirect

BBA - Molecular Basis of Disease

journal homepage: www.elsevier.com/locate/bbadis

Absence of MMACHC in peripheral retinal cells does not lead to an ocular phenotype in mice

Eva Kiessling [a], Sarah Nötzli [a], Vyara Todorova [a], Merima Forny [b,1], Matthias R. Baumgartner [b], Marijana Samardzija [a], Jakub Krijt [c], Viktor Kožich [c], Christian Grimm [a,*,2], D. Sean Froese [b,2,*]

[a] Lab for Retinal Cell Biology, Dept. Ophthalmology, University Hospital Zurich, University of Zürich, Switzerland
[b] Division of Metabolism and Children's Research Center, University Children's Hospital Zürich, University of Zürich, Switzerland
[c] Dept. of Pediatrics and Inherited Metabolic Disorders, Charles University-First Faculty of Medicine and General University Hospital, Prague, Czech Republic

ARTICLE INFO

Keywords:
cblC deficiency
Mmachc deficiency
Retina
Vitamin B12 deficiency
Ocular phenotype

ABSTRACT

Combined methylmalonic aciduria with homocystinuria (cblC type) is a rare disease caused by mutations in the *MMACHC* gene. *MMACHC* encodes an enzyme crucial for intracellular vitamin B_{12} metabolism, leading to the accumulation of toxic metabolites *e.g.* methylmalonic acid (MMA) and homocysteine (Hcy), and secondary disturbances in folate and one-carbon metabolism when not fully functional. Patients with cblC deficiency often present in the neonatal or early childhood period with a severe multisystem pathology, which comprises a broad spectrum of treatment-resistant ophthalmological phenotypes, including retinal degeneration, impaired vision, and vascular changes. To examine the potential function of MMACHC in the retina and how its loss may impact disease, we performed gene expression studies in human and mouse, which showed that local expression of *MMACHC* in the retina and retinal pigment epithelium is relatively stable over time. To study whether functional MMACHC is required for retinal function and tissue integrity, we generated a transgenic mouse lacking *Mmachc* expression in cells of the peripheral retina. Characterization of this mouse revealed accumulation of cblC disease related metabolites, including MMA and the folate-dependent purine synthesis intermediates AICA-riboside and SAICA-riboside in the retina. Nevertheless, fundus appearance, morphology, vasculature, and cellular composition of the retina, as well as ocular function, remained normal in mice up to 6 or 12 months of age. Our data indicates that peripheral retinal neurons do not require intrinsic expression of *Mmachc* for survival and function and questions whether a local MMACHC deficiency is responsible for the retinal phenotypes in patients.

1. Introduction

Methylmalonic aciduria and homocystinuria, cblC type (OMIM: #277400), is a rare disease caused by mutations in the *MMACHC* gene, with around 500 patients diagnosed worldwide [1]. Patients typically present in the infantile period (<1 year) with failure to thrive, metabolic acidosis, thrombotic microangiopathy, and neurological symptoms such as lethargy, developmental delay, and muscular hypotonia [2], often with additional megaloblastic anemia or neutropenia/pancytopenia [3,4].

This early severe presentation is particularly associated with the c.271dupA (p.Arg91Lysfs*14) variant, which is frequently identified in European and North American patients and accounts for ~40% of disease alleles [2,5]. Biochemically, patients with the cblC defect are characterized by an accumulation of methylmalonic acid (MMA) and total homocysteine (Hcy) in body fluids, reflecting deficiency of the vitamin B_{12} (cobalamin, Cbl) dependent enzymes methylmalonyl-CoA mutase and methionine synthase, respectively, often accompanied by low levels of methionine (Met), S-adenosylmethionine (SAM), and glutathione [6–8]. Treatment includes parenteral administration of hydroxocobalamin (OHCbl) and oral supplementation of betaine, folinic acid, and L-carnitine, in most cases resulting in a decline of toxic metabolites and reduced incidence of acute crises and non-neurological symptoms [3,9].

Especially patients with an early disease onset frequently show a number of heterogeneous ophthalmic manifestations such as

* Corresponding authors.
E-mail addresses: cgrimm@opht.uzh.ch (C. Grimm), sean.froese@kispi.uzh.ch (D.S. Froese).
[1] Present address: Institute for Regenerative Medicine (IREM), University of Zurich, Switzerland.
[2] Equal contribution.

https://doi.org/10.1016/j.bbadis.2021.166201
Received 9 March 2021; Received in revised form 25 May 2021; Accepted 8 June 2021
Available online 17 June 2021
0925-4439/© 2021 The Author(s). Published by Elsevier B.V. This is an open access article under the CC BY license (http://creativecommons.org/licenses/by/4.0/).

degeneration of the central retina, bull's eye atrophy, and impaired photopic vision (impaired cone function). Additionally, chorioretinal atrophies, optic nerve pallors, vessel attenuation as well as nystagmus, strabismus, and even optic colobomas have been observed [2,10–17]. Due to newborn screening programs, patients now have the chance to be diagnosed and treated early after birth. Even though treatment success is variable, patients' life span is significantly prolonged in most cases [18,19]. Unfortunately, however, the ocular phenotype does not respond to current treatments and often leads to severe visual impairment that can progress to legal blindness [20]. This observation has led to the hypothesis that retinal cells may require intrinsic MMACHC activity for survival and function.

When vitamin B_{12} is ingested as a nutrient, it must undergo certain absorption and processing steps. A protein known as intrinsic factor (IF) binds the free Cbl until this complex has reached the terminal ileum [21,22]. Here, IF-Cbl is recognized by distinct cells of the mucosa with the help of a receptor consisting of a heterodimer of amnionless and cubilin, also referred to as CUBAM [21,23]. Cellular absorption of Cbl *via* endocytosis is facilitated by transcobalamin II (TCII), which binds Cbl, and the transcobalamin receptor (TCblR/*CD320*) [21,24]. In the cell, the cytosolic MMACHC protein is responsible for the proper transport and processing of Cbl [25] and acts as a dual-function enzyme. It binds incoming Cbl molecules, decyanates or dealkylates, and sorts them to downstream target enzymes [25–27]. To function as an active cofactor for essential enzymatic reactions, the resulting Cbl is either adenosylated (AdoCbl) or methylated (MeCbl) [27–30]. AdoCbl is required by methylmalonyl-CoA-mutase (MMUT), which is located in the mitochondria and converts *L*-methylmalonyl-CoA to succinyl-CoA. Succinyl-CoA enters the Krebs cycle where it serves as an important intermediate in the catabolism of odd-chain fatty acids and branched-chain amino acids. An interruption of this step, through dysfunction of MMUT or failed production of AdoCbl, results in accumulation of its substrate methylmalonyl-CoA converted to free MMA [31]. By contrast, MeCbl is needed by the cytosolic enzyme methionine synthase (MS), encoded by 5-methyltetrahydrofolate-homocysteine methyltransferase (*MTR*), which recycles homocysteine back to methionine and releases tetrahydrofolate for proper functioning of the one-carbon metabolism. Methionine is then further converted into SAM, which represents the most important methyl group donor for DNA methylation as well as a host of other reactions. Dysfunction of MS, including through deficiency of its cofactor MeCbl, results in lower levels of methionine and sometimes SAM, as well as accumulation of Hcy. Moreover, the functional block at the level of MS leads to accumulation of methyltetrahydrofolate (known as the methyl folate trap), lack of tetrahydrofolate, and secondary disturbances in one-carbon metabolism responsible for megaloblastic anemia, for example. Since both AdoCbl and MeCbl synthesis are dependent on MMACHC, MMUT and MS function is disrupted in cblC deficiency [28,32,33].

Compared with cblC patients, those with isolated methylmalonic aciduria caused by mutations in *MMUT* present with higher plasma and urine concentrations of MMA [13,34–36]; while many patients suffering from classical homocystinuria (caused by dysfunction of cystathionine beta-synthase) have higher plasma total Hcy (tHcy) concentrations [13,37]. Nevertheless, neither of those patient groups displays an ocular phenotype similar to cblC patients. This may indicate that the metabolites do not efficiently reach the retina even though Hcy was reported to affect the inner and outer blood-retinal barrier [38], that the increased presence of a single metabolite is not sufficient to develop a severe retinal phenotype, or that retinal cells indeed require an intrinsic function of MMACHC, as suggested above.

Very few animal models are available to study the ocular phenotype of cblC deficiency. Moreno-Garcia et al. [39] generated a systemic knockout of *Mmachc* in mice, which turned out to be embryonically lethal, preventing post-natal investigations of potential ocular phenotypes. A recent publication by Sloan et al. [40] reported a viable *mmachc* knockout in zebrafish. Besides methylmalonic acidemia and severe growth retardation, these fish also displayed thinning of the optic nerve, photoreceptors with shortened outer segments, and loss of some photoreceptors leading to a reduced thickness of the outer retina 28 days post fertilization. Chern et al. [41] generated two transgenic mouse lines with either a loss of function (conditional *Mmachc* null) or a gain of function (*Mmachc* overexpression). They confirmed the embryonal lethality of *Mmachc* null mice and described the embryos to be an- or microophthalmic [41]. Due to the high lethality and pleiotropy in systemic *Mmachc* knockouts, conditional knockout models are needed to investigate the mechanisms underlying tissue-specific pathologies of MMACHC deficiency. To test whether *Mmachc* holds an essential local function in retinal cells that could explain not only the ocular phenotype but also the resistance to therapy in patients, we generated a mouse model (retina$^{\Delta Mmachc}$) that lacks functional *Mmachc* in most cells of the retina. Although these cells are knockout for *Mmachc*, the retina as a whole has to be considered a knockdown-tissue as some cells still express the functional wild-type gene. Nevertheless, these mice enable examination of whether retinal cells require intrinsic MMACHC activity for function and survival.

2. Methods

2.1. Animals and generation of the retina$^{\Delta Mmachc}$ mouse model

Male and female mice were used in this study. All mice, including Balb/c wild-type (wt) mice (purchased from Charles River, Calco, Italy), were maintained at the laboratory animal service center (LASC) of the University of Zurich under a 14/10 h light/dark cycle with food and water *ad libitum*. Mice were euthanized by CO_2 followed by beheading. All experiments were approved by the veterinary authorities of canton Zurich, Switzerland (Project Identification Number: ZH141/16 and ZH091/19) and adhered to the ARVO statement for the use of animals in ophthalmic and vision research.

Mmachc$^{flox/flox}$ mice (C57BL/6N) were generated at PolyGene (Rümlang, Switzerland). The sequence of the wt *Mmachc* genomic DNA (NCBI gene ID: 67096) was modified to carry a neomycin resistance (neo) gene flanked by two FRT sites in intron 2, a loxP site upstream of the 5′ FRT site (146 bp upstream of exon 3) and a loxP site in the 3′UTR of exon 4 (220 bp downstream of the STOP codon). The neomycin resistance gene was deleted using *in vivo* Flp recombination by a deleter strain leading to the final *Mmachc*$^{flox/flox}$ mouse. For detailed sequence information, see supplemental information.

Knockout of *Mmachc* in cells of the developing retina was achieved by crossing *Mmachc*$^{flox/flox}$ mice with mice expressing Cre recombinase under the control of the α-element of the *Pax6* promoter restricting Cre expression to retinal progenitor cells that develop into neurons of the peripheral but not central retina or the RPE [42]. Thus, excision of exons 3 and 4 of the *Mmachc* gene was limited to the peripheral neuronal retina leaving cells of central retinal area stretching to about 600 μm to either side of the optical disc unaffected (see Fig. 1a of [43]). *Mmachc*$^{flox/flox}$; *Pax6Cre* mice are referred to as retina$^{\Delta Mmachc}$ mice. *Mmachc*$^{flox/flox}$ mice served as controls.

2.2. Electroretinography (ERG)

Mice were dark-adapted overnight. Prior to ERG recording, pupils were dilated with 1% cyclogyl (Alcon Pharmaceutical, Cham, Switzerland) and 5% phenylephrine (Ciba Vision, Niederwangen, Switzerland). Mice were anaesthetized with a subcutaneous injection of a mixture of Ketamine (85 mg/kg, Parke-Davis, Berlin, Germany) and Rompun (Xylazine, 10 mg/kg, Bayer AG, Leverkusen, Germany) and kept on a heated pad to maintain body temperature at 37 °C. Golden ring electrodes were placed onto each cornea. Mice were exposed to light flashes ranging from −50 dB (0.000025 cd*s/m^2) to 15 dB (79 cd*s/m^2) for scotopic and from −10 dB (25 cd*s/m^2) to 25 dB (790 cd*s/m^2) for photopic ERG. Mice were light-adapted for 5 min prior to photopic ERG

recordings. Light-evoked retinal responses were measured with an LKC UTAS Bigshot unit (LKC Technologies, Inc. Gaithersburg, MD, USA). For each light intensity, 10 recordings were averaged.

2.3. Fundus imaging, optical coherence tomography (OCT) and angiography

Dilation of pupils and anesthesia were performed as described above. To keep the eyes moist 2% methocel (OmniVision AG, Neuhausen, Switzerland) was applied. Mice were placed on a holder and fundus images and OCT scans were acquired using the Micron IV system (Phoenix Research Labs, Pleasanton, CA, USA). For fluorescein angiography mice were injected intraperitoneally with 50 μL of 2% fluorescein solution (Novartis AG, Basel, Switzerland) and ocular vasculature was imaged using the same equipment.

2.4. Retina and eyecup isolation

The corneas of euthanized mice were opened using a sharp scalpel. Lens and vitreous were removed through the opening, and the neural retina was harvested using curved tissue forceps and snap frozen in liquid nitrogen. The remaining eyecup representing the RPE was isolated from the eye socket using scissors and frozen in liquid nitrogen. Whole retina and whole eyecup samples were used for PCR, qPCR and metabolomics.

2.5. Human retina and RPE

Isolation and analysis of eye bulbs from post-mortem donors at the University Hospital of Zurich was approved by the ethics committee of canton Zurich, Switzerland (BASEC-Nr: PB_2017-00550) and adhered to the tenets of the Declaration of Helsinki.

Donor age ranged from 17 to 91 years. Age, gender, and known diseases of donors are listed in Supplementary Table 1. After removal of the cornea, eyeballs were immersed in PBS and cut into a clover-leaf structure. Lens and vitreous were removed and nasal mid-peripheral and central retina dissected. Retina and RPE samples from these regions were isolated separately, snap-frozen and stored in liquid nitrogen until use. RNA isolation and cDNA synthesis were performed as described below.

2.6. Genomic DNA isolation from mouse tissue

Genomic DNA (gDNA) was isolated by immersing whole retinas in 200 μL of 1× tissue homogenization buffer (500 mM KCl, 100 mM Tris-HCl (pH 8.3), 0.1 mg/mL Gelatin, 0.45% Nonidet P-40, 0.45% Tween 20) containing 50 mg/mL Proteinase K (Sigma-Aldrich, Buchs SG, Switzerland) and shaking for 30 min at 55 °C. Proteinase K was deactivated at 95 °C for 10 min followed by a centrifugation step at 10,000 rcf for 5 min. The supernatant containing genomic DNA was used for PCR.

2.7. Genotyping and detection of Mmachc deletion fragment

Mice were genotyped using 2 μL of genomic DNA, the GoTaq Green Master Mix from Promega (Dübendorf, Switzerland), specific primer pairs (Supplementary Table 2), and the following PCR conditions: initial denaturation (95 °C, 5 min); 35 cycles of denaturation (95 °C, 45 s), annealing (60 °C, 45 s) and elongation (72 °C, 45 s); final extension (72 °C, 10 min). To assess excision of the floxed sequence in *Mmachc*, PCR was performed using the same parameters but with the elongation time set to 3 min and primers spanning E3 and E4 (Supplementary Table 2, Fig. 2).

2.8. RNA isolation, cDNA synthesis and real-time PCR

Total RNA was isolated from whole mouse retinas using the NucleoSpin RNA kit (Macherey-Nagel, Oensingen, Switzerland), while RNA from human donor samples was purified with the RNeasy Mini Kit (Qiagen, Hilden, Germany) following the manufacturer's instructions. Mouse retina and eyecups were homogenized by thoroughly pipetting the tissue through a 21G needle. Nonhomogenized material in eyecup samples was removed prior to RNA isolation to avoid clogging of spin column membranes. cDNA was synthesized from 1 μg of RNA using oligo-dT primers and M-MLV reverse transcriptase (Promega) and adjusted to 5 ng/μL. Relative transcript levels of specific genes were determined by semi-quantitative real-time PCR (qPCR) using 10 ng of cDNA, PowerUp SYBR Green master mix (Thermo Fisher Scientific, Waltham, MA, USA), and respective primer pairs (Supplementary Table 2) on an ABI QuantStudio3 qPCR device (Thermo Fisher Scientific, Waltham, MA, USA). Expression levels were normalized to *Actb* for mouse genes or to *RPL28* for human genes, and relative expression was calculated using the ΔΔCt method [44] using Thermo Fisher Scientific Cloud Software (Thermo Fisher Scientific).

2.9. Immunofluorescence

Following euthanasia, eyes were marked nasally using a small heated metal pen, enucleated and fixed in 4% paraformaldehyde (PFA) in 0.1 M phosphate buffer at 4 °C. After 1 h, the cornea was opened with scissors and eyes incubated for an additional hour in PFA. After removal of the lens, eyes were post-fixed for 2 h in 4% PFA at 4 °C, immersed in 30% sucrose for 1 h and embedded in aluminum molds filled with tissue freezing medium (O.C.T., Leica Biosystems Nussloch GmbH, Nussloch, Germany). Then the aluminum molds were placed in a liquid-nitrogen-cooled 2-methylbutane bath (Sigma-Aldrich, Buchs SG, Switzerland) to solidify the O.C.T. Blocks were stored at −80 °C until sectioning. Cryosections (12 μm) containing the optic nerve head were blocked for 1 h at room temperature in blocking solution (3% normal goat serum (Sigma-Aldrich, St. Louis, MO, USA), 0.3% Triton X-100 (Sigma-Aldrich, Buchs SG, Switzerland)), after which sections were incubated with primary antibodies (Supplementary Table 3) overnight at 4 °C. Following three wash steps with phosphate-buffered saline, sections were incubated with secondary antibodies (Supplementary Table 3) for 1 h at room temperature and nuclei were counterstained with DAPI (4′,6-Diamidine-2′-phenylindole dihydrochloride, Roche, Basel, Switzerland). Fluorescence was analyzed by fluorescence microscopy (Axioplan 2, Zeiss, Feldbach, Switzerland).

2.10. Morphology

Nasally marked eyes were enucleated and fixed overnight at 4 °C in 2.5% glutaraldehyde/0.1 M cacodylate buffer. Cornea and lens were removed, and a cut was made through the optic nerve head to separate the eye into nasal and temporal halves. Tissue was washed in cacodylate buffer (0.1 M, pH 7.2) and fixed for 1 h at room temperature in 1% osmium tetroxide (in cacodylate buffer). Following dehydration in increasing ethanol concentrations, tissue was embedded in Epon blocks (Sigma-Aldrich, Buchs SG, Switzerland), cut into 0.5 μm thick sections, counterstained with toluidine blue, and analyzed by light microscopy with the Axioplan 2 microscope (Axioplan 2, Zeiss).

2.11. In situ hybridization

Enucleated eyes were fixed in 4% PFA in 0.1 M phosphate buffer for 24 h at RT. A small portion on one side of the eye was removed to enable paraffin penetration. Then, eyes were dehydrated in 90% ethanol and xylene, embedded into paraffin molds, and cut into 5 μm thick sections.

The RNAscope 2.5 HD Red Detection Kit (Cat. No. 322350, Advanced Cell Diagnostics, Newark, CA, USA) was used for *in situ* hybridization

and detected by fluorescent and light microscopy according to the manufacturer's protocol with the following modifications: Incubation times for target retrieval (15 min), protease treatment (20 min) and signal detection (25 min) were adapted to optimize signal-to-noise ratio for retinal tissue. The probe to detect mouse *Mmachc* mRNA (Mmachc-01) was custom-designed to bind to exons 3 and 4 (344–800 bp) of *Mmachc*, based on Gene ID 67096 and NCBI Reference Sequence: NM_025962.3. The probe *dapB* (Cat No. 310043), specific for bacterial *L*-2,3-dihydrodipicolinate reductase, served as a negative control.

2.12. Metabolite determination in retinal tissue

Metabolites were determined in three control and three retina$^{\Delta Mmachc}$ samples. Each sample contained 10 to 14 individual retinas collected from up to 7 age-matched mice. Pooling of retinas was required to reach 50 mg of tissue per sample needed for analysis. Thus, data collected correspond to 30 to 40 retinas per group. Isolated retinas were weighed and homogenized using tissue raptor homogenizer (Qiagen, Hilden, Germany) in 3 μL/mg of a buffer containing 1% lauryl maltoside in 100 mM Tris, pH 8.5. The homogenates were incubated for 20 min in a water/ice bath, sonicated by a microtip (5 cycles, each cycle 3 s) using a 4710 Series Ultrasonic Homogenizer (Cole-Parmer Instrument Co., Chicago, Illinois, USA) and centrifuged at 4 °C at 15,000*g* for 20 min. The supernatant was aliquoted and stored at −80 °C prior to metabolite analyses.

Previously published LC-MS/MS methods were used for the determination of S-adenosylmethionine (SAM) and S-adenosylhomocysteine (SAH) [45], taurine, hypotaurine and methylated glycines [46] and 5-aminoimidazole-4-carboxamide riboside (AICA-riboside) and 5-amino-4-imidazole-N-succinocarboxamide riboside (SAICA-riboside)[47]. Commercially available kits were used for LC-MS/MS determination of amino acids methionine, glycine, serine and thioethers cystathionine and lanthionine (EZ:faast, Phenomenex, Torrance, USA) and for determination of MMA (ClinMass® Komplettkit, advanced, RECIPE Chemicals + Instruments, GmbH, München, Germany).

All LC-MS/MS methods were performed on an Agilent 1290 Infinity LC System (Agilent Technologies, Palo Alto, CA, USA) coupled with an API 4000 triple quadrupole mass spectrometer with an electrospray ion source. Detection of analytes was carried out using positive electrospray ionization technique and selected multiple reaction monitoring.

Total aminothiols (cysteine, cysteinylglycine, homocysteine, glutathione and γ-glutamylcysteine) were determined by reversed-phase HPLC with fluorescent detection (Shimadzu LC-20AD system with RF-20AXs fluorescence detector, Shimadzu Corporation, Kyoto, Japan) after derivatization with ammonium 7-fluorobenzo-2-oxa-1,3-diazole-4-sulfonate (SBD-F). The reduction of disulfides and protein bound aminothiols was performed with tris(2-carboxyethyl)phosphine (TCEP) as described previously [48,49].

2.13. Statistical analysis

All statistical analyses were done with the PRISM software V.8 (Graphpad Software, San Diego, CA, USA). Significance tests for the individual results are stated in the figure legends.

3. Results

3.1. MMACHC is expressed in human and mouse retina and RPE

Since treatment of cblC deficiency does not improve the retinal phenotype of patients, a local role of MMACHC in the retina was suspected. To examine the expression pattern of *MMACHC* in the eye, we performed qPCR on cDNA prepared from retina and RPE of human donors and C57BL/6 wild type mice. Expression of *MMACHC* was stable in the peripheral and central (including the macula) adult human retina, as well as in the central RPE, but showed a slight decline in the peripheral RPE during aging (17–91 years) (Fig. 1A). Mouse retina and eyecup (representing the RPE) expressed *Mmachc* without strong age-dependent alterations in expression in the adult animals after 1 month and up to 1 year of age, which corresponds roughly to 50-years in human age [50]. During post-natal development (up to 1 month of age), however, *Mmachc* expression gradually increased in the retina. Somewhat in contrast, *Mmachc* expression in the eyecup was higher at two early timepoints (1 day and 7 days) before it remained at slightly reduced levels in the adult mouse after 1 month of age (Fig. 1B). *In situ* hybridization of ocular sections from a wild type BALB/c mouse revealed that *Mmachc* was not only expressed in all layers of the retina and in the RPE, but was also present in the lens epithelium, corneal *endo*- and epithelium, and ciliary body (Fig. S1). The expression pattern supported local expression of *MMACHC* and a potential functional significance of the protein in the retina.

3.2. Pax6-Cre mediated excision of floxed Mmachc sequences results in a significant reduction of Mmachc expression in the peripheral mouse retina

To investigate a possible function of MMACHC in retinal cells, we generated a retina-specific *Mmachc* knockdown mouse (retina$^{\Delta Mmachc}$). This was achieved by crossing a novel transgenic mouse carrying *loxP* sequences flanking exons 3 and 4 of *Mmachc* (Fig. 2A) with *Pax6-Cre* mice that express Cre recombinase in retinal progenitors starting at embryonic day E10.5 [42]. This leads to the recombination of *loxP* sites in cells forming the peripheral retina, but not the central retina or RPE [42], as early as post-natal day 1 [43,51]. Data from reporter mice indicates that cells in a retinal area of an estimated 70% undergo Cre-mediated recombination (see Fig. 1A of [51] and Fig. 1A of [43]). Recombination of the *loxP* sites in *Mmachc* deletes exons 3 and 4, including the stop codon. Thus, a potentially expressed truncated mRNA encodes the N-terminal 91 aa but lacks the C-terminal 188 aa of the MMACHC protein. The deletion of the floxed sequence in mice resembles the molecular consequences of the frequent and phenotypically severe c.271dupA (p.Arg91Lysfs*14) variant in humans, which leads to a truncated protein containing only the N-terminal 90 aa of MMACHC [5,33].

To test for deletion, we performed conventional PCR with primers targeting intron 2 and the 3′ untranslated region of exon 4 (Fig. 2A) using genomic DNA isolated from whole retinas isolated from control and retina$^{\Delta Mmachc}$ mice. PCR yielded a fragment of 2769 bp (unexcised) in control mice and the expected fragment of 729 bp (excised) in retina$^{\Delta Mmachc}$ mice (Fig. 2B). This confirmed a successful deletion of exons 3 and 4 in retinal tissue of retina$^{\Delta Mmachc}$ mice (Fig. 2B). Since cells in the central retina do not recombine the floxed sequence and contain the wild type gene (see above), the almost complete absence of the long unexcised fragment was likely due to the more efficient amplification of the shorter deletion fragment under our experimental conditions. As shown by others [42], Cre expression was confirmed to be specific for the neuronal retina (Fig. 2C). The minimal Cre expression detected in eyecup samples (Fig. 2C) likely resulted from minor contaminations of the eyecup with neuronal retina during tissue isolation and separation. qPCR using primer pairs amplifying exons 2 and 3 showed that *Mmachc* mRNA expression was reduced by 75% in the retina but not in the eyecup of retina$^{\Delta Mmachc}$ mice (Fig. 2D). This reduction corresponded nicely to the estimated retinal area (70%) where Cre recombinase was active (see above). Interestingly, when using primers that were designed to bind to the first two exons of *Mmachc*, upstream of the *loxP* sites, we found that *Mmachc* transcript levels were only decreased by 50% in retina$^{\Delta Mmachc}$ mice (Fig. 2D). This suggests that cells with successful *Mmachc* recombination produced a shortened transcript, albeit at reduced levels. However, if such an RNA was translated, the resulting truncated protein would contain maximally the N-terminal 91 aa of MMACHC and thus should lack enzymatic activity [52,53].

Finally, *in situ* hybridization showed that the central retina of retina$^{\Delta Mmachc}$ mice had a signal distribution resembling that of control mice,

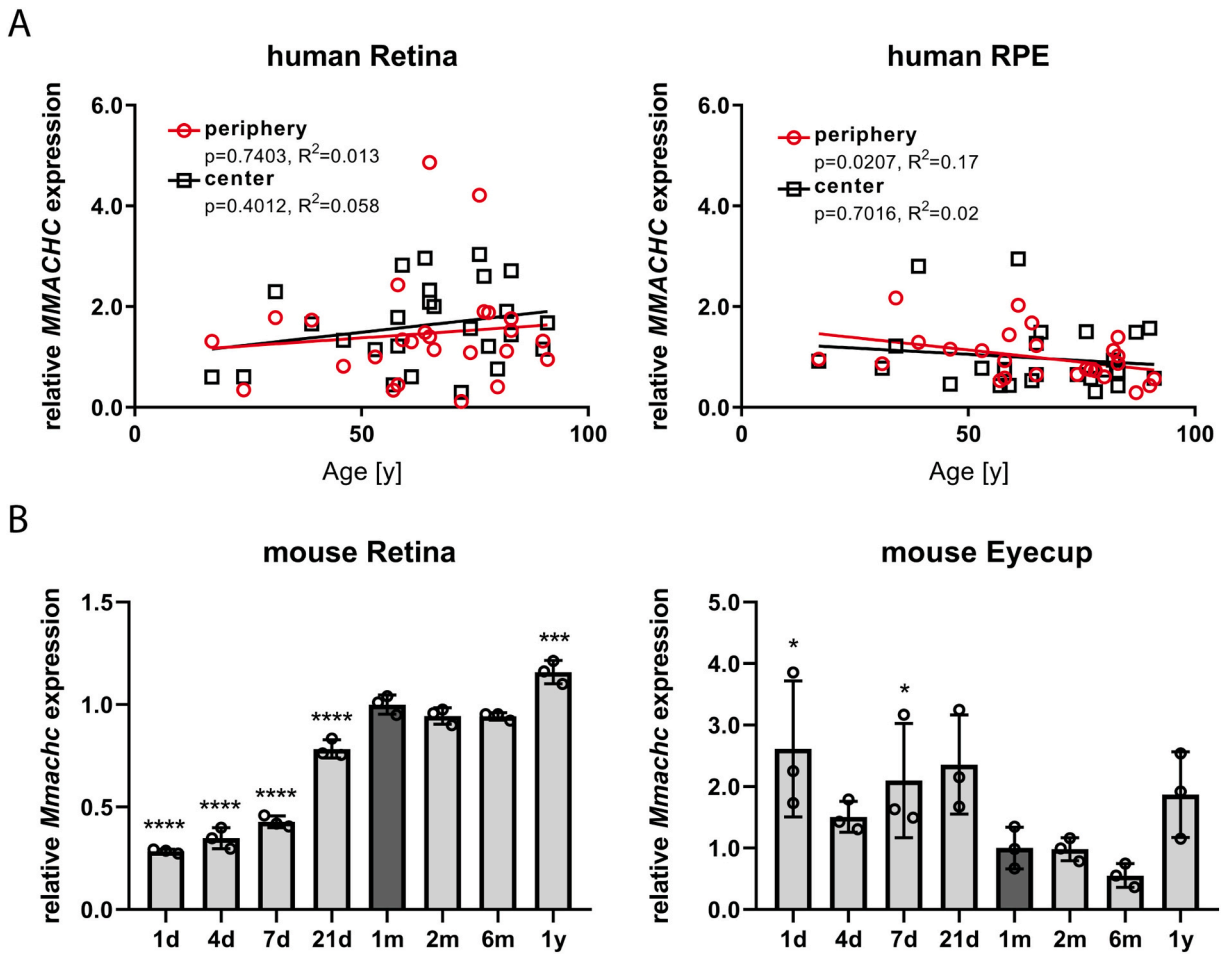

Fig. 1. Expression of *MMACHC* in the human and mouse neural retina and RPE. A) Relative *MMACHC* mRNA levels in the peripheral (red circles) and central (black squares) retina (left) and RPE (right) of human donor eyes without diagnosed eye disease. Each data point represents mRNA expression levels plotted against age. Statistical analysis was performed using linear regression. The linear regression trend line is shown. $n = 27$. B) Relative *Mmachc* mRNA levels in the wild type mouse retina (left) and eyecup (right) during postnatal development and aging. Abbreviations: d, day; m, month; y, year. One month of age was chosen as the reference time point and set to 1. Shown are individual data points and means ± SD, $n = 3$. Statistical analysis was performed using One-way ANOVA with Dunnet's multiple comparisons tests comparing all time points to the reference time point. * = $p < 0.05$, *** = $p < 0.001$, **** = $p < 0.0001$.

whereas the peripheral retina was almost completely devoid of *Mmachc* mRNA (Fig. 2E). Together, these data indicate an efficient *Mmachc* knockout in cells of the peripheral retina in retina$^{\Delta Mmachc}$ mice.

3.3. Metabolites associated with cblC deficiency are elevated in retinas of retina$^{\Delta Mmachc}$ mice

To determine whether retinas of retina$^{\Delta Mmachc}$ mice showed evidence of MMACHC dysfunction, we performed a targeted metabolomic analysis of compounds relevant to cblC deficiency (Table 1). Similar to the altered metabolite levels in the serum of patients, retinas of retina$^{\Delta Mmachc}$ mice had a significant 5.6-fold increase in MMA. Even though a slight tendency to an increase was noted, Hcy levels did not change significantly. Moreover, we found AICA-riboside and SAICA-riboside, two dephosphorylated derivatives of *de novo* purine synthesis intermediates, to be significantly increased by 22.3-fold and 11.5-fold, respectively. These purine compounds may be elevated due to a putative depletion of 10-formyltetrahydrofolate caused by the methyl folate trap. Finally, we found nearly all investigated intermediates of transsulfuration to be reduced, whereby cysteinylglycine, cysteamine and glutathione were reduced by approximately 50% (Table 1).

3.4. Retina$^{\Delta Mmachc}$ mice have normal retinal function

Several reports have shown that *cblC* deficient patients suffer from impaired visual function, often in the photopic response to light [10–13,15,16]. To test whether the inactivation of *Mmachc* in retinal cells resulted in a similarly affected function in mice, we recorded scotopic and photopic ERGs from 24-week old mice. We found that the forms and amplitudes of a-waves (negative deflection) and b-waves (positive deflection) of the scotopic responses and the b-waves of the photopic responses did not differ between control and retina$^{\Delta Mmachc}$ mice (Fig. 3). This indicates that neither the rod (scotopic) nor the cone (photopic) system was affected by the lack of *Mmachc* in retinal cells and suggests that MMACHC activity may not be required for retinal function in mice.

3.5. Retina$^{\Delta Mmachc}$ mice show no morphological abnormalities

It has been reported that *cblC* patients show changes in fundus appearance, such as retinal atrophy, central pigmentary clumping, and vessel attenuation [15,16]. We used fundus imaging, OCT, and fluorescence angiography to examine retinal integrity of retina$^{\Delta Mmachc}$ mice at 24 weeks of age. Fundus photography as well as fluorescein angiography allow a macroscopic view of the retina and retinal vessel architecture. While angiography is a standard procedure to assess the

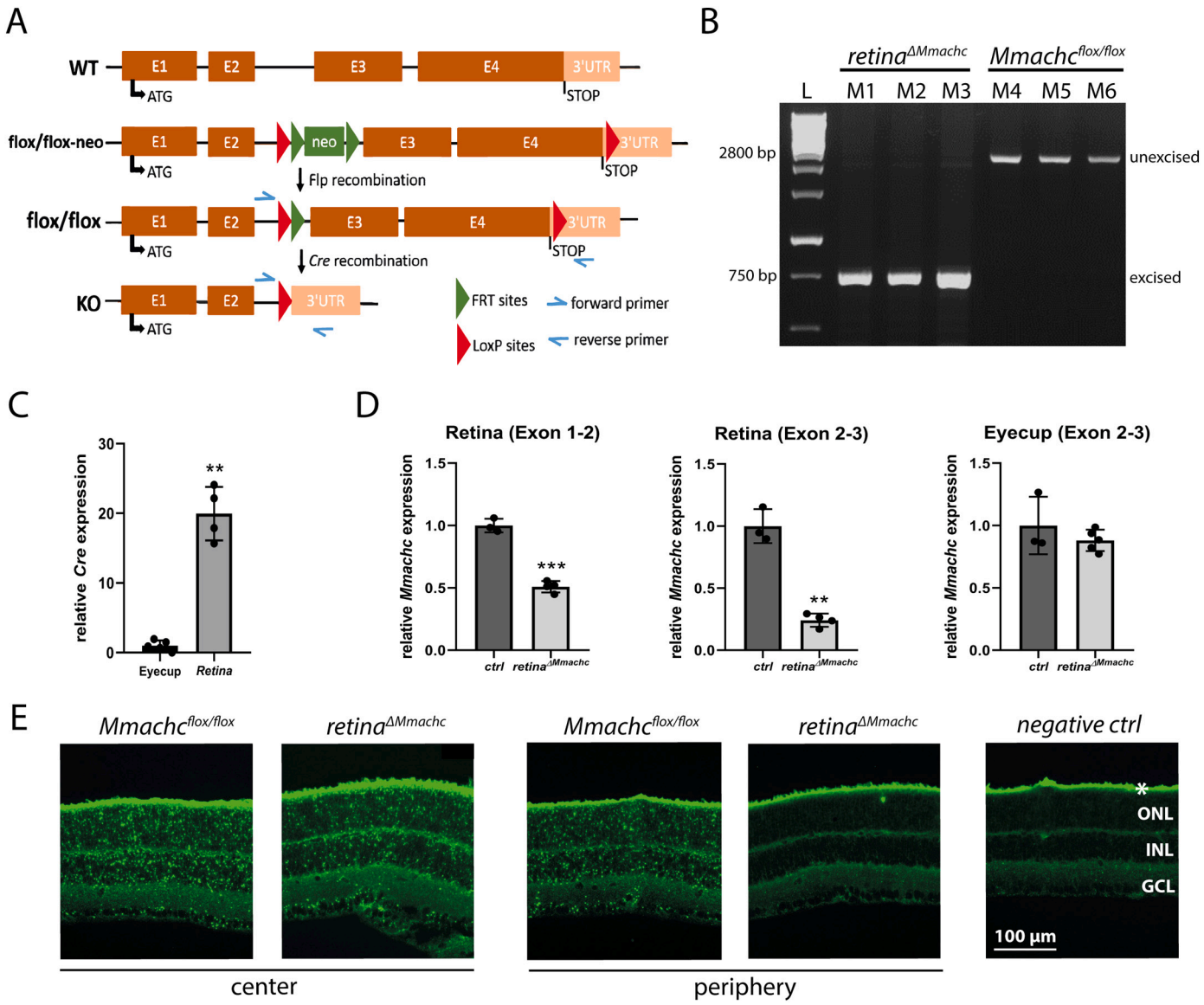

Fig. 2. Reduced retinal expression of *Mmachc* in *retina*$^{\Delta Mmachc}$ mice. A) Generation of the retina$^{\Delta Mmachc}$ mouse model. Schematic representation of the wild type (WT) *Mmachc* allele with exons 1–4 (E1–E4, brown) including the 3′ UTR (light brown). The flox/flox-neo targeting vector contained a pair of *loxP* sites (red triangles) flanking exons 3 and 4 (including STOP codon) and a pair of flippase recognition target (FRT) sites (green triangles) flanking the neomycine cassette. The final flox/flox allele of *Mmachc* was obtained after the *in vivo* removal of FRT-flanked neomycin selection cassette using a Flp-deleter strain. *Mmachc*$^{flox/flox}$ mice were crossed with Pax6-Cre mice leading to the recombination of the *loxP* sites and deletion of E3 and E4 and thus to a *Mmachc* knockout (KO). The positions of primers used for genotyping are indicated with arrows. B) Confirmation of successful deletion of exons 3 and 4 of the *Mmachc* gene in three retina$^{\Delta Mmachc}$ (M1–M3) but not three control *Mmachc*$^{flox/flox}$ (M4–M6) mice by PCR. A DNA fragment of 2769 bp represents the unexcised floxed allele, while a 729 bp fragment indicates the excised allele. L, DNA ladder. C) *Cre* expression in the retina and eyecup of *Cre*-positive mice by semiquantitative real-time PCR. ($n = 4$). D) Relative expression levels of *Mmachc* using primers binding to exons 1–2 or exons 2–3 (as indicated) in the retina (left and middle panel) and eyecup (right panel) of retina$^{\Delta Mmachc}$ (light grey; $n = 4$) and control mice (dark grey; $n = 3$). The mRNA levels in controls were set to 1. Shown are individual data points and means ± SD. Statistics: unpaired *t*-test with Welch's correction. ** = $p < 0.005$, *** = $p < 0.001$. E) Representative images of *in situ* hybridization to detect *Mmachc mRNA* (exon 3–4 specific probes) in the central and peripheral retinas of *Mmachc*$^{flox/flox}$ and retina$^{\Delta Mmachc}$ mice at 6 weeks of age. Negative ctrl represents hybridization with bacterial dapB. *: autofluorescent photoreceptor segments. RPE not present. Scale bar as indicated. ONL: outer nuclear layer, INL: inner nuclear layer, GCL: ganglion cell layer.

integrity of the retinal vasculature, OCT imaging provides a non-invasive method to register retinal and optic nerve head pathophysiologies [54]. No obvious differences were identified in the appearance of ocular fundi, and angiography showed no vessel leakage and no indication of hypo- or hypervascularization in retina$^{\Delta Mmachc}$ mice (Fig. 4A). Similarly, OCT images revealed well distinguishable and normal retinal layers in the central and more peripheral retina (Fig. 4A), suggesting that the absence of *Mmachc* did not lead to gross retinal alterations.

Since subtle changes in retinal morphology are challenging to detect with *in vivo* imaging methods, we used light microscopy of semi-thin retinal sections for a detailed analysis of retinal structures at 4, 24, and 52 weeks of age (Fig. 4B). Similar to OCT data, retinal sections from the center (Fig. 4B, upper panels) and the periphery (Fig. 4B, lower panels) did not provide evidence of morphological changes in retina$^{\Delta Mmachc}$ mice, as is indicated by the normal appearance of the photoreceptor segments and the outer and inner nuclear layers. This was corroborated by outer nuclear layer (ONL) thickness spidergrams, which showed no significant differences between control and retina$^{\Delta Mmachc}$ mice at all ages tested (Fig. 4B).

Table 1
Concentration of metabolites in retinas of three *Mmachc*$^{flox/flox}$ (CTL) and three retina$^{\Delta Mmachc}$ (KO) mice. AVG: average (mean). Statistics: Unpaired *t*-test with Welch's correction.

	KO/CTL Fold change	µmol/g protein							
		CTL 1	CTL 2	CTL 3	AVG	KO 1	KO 2	KO 3	AVG
Ado-cbl related metabolites									
Methylmalonic acid (MMA)	**5.62***	0.016	0.013	0.019	**0.016**	0.091	0.067	0.109	**0.089**
Transmethylation related metabolites									
Total homocysteine (tHcy)	**1.63**	0.0080	0.0079	0.0072	**0.0077**	0.0087	0.0149	0.0140	**0.0125**
Methionine (Met)	**0.76**	1.287	1.044	0.772	**1.03**	0.669	0.702	0.981	**0.784**
Met/tHcy ratio	**0.47**	160.88	132.15	07.22	**134.30**	76.90	47.11	70.07	**62.53**
S-adenosylmethionine	**1.52**	0.0478	0.0318	0.0459	**0.0418**	0.080	0.021	0.090	**0.064**
S-adenosylhomocysteine	**1.27**	0.0218	0.0252	0.0262	**0.0244**	0.025	0.031	0.037	**0.031**
Transsulfuration related metabolites									
Cystathionine	**0.84**	0.032	0.034	0.086	**0.051**	0.018	0.043	0.067	**0.043**
Total cysteine	**0.86**	14.3	11.8	12.7	**13.0**	9.6	9.4	14.6	**11.2**
Lanthionine	**0.61**	0.0036	0.0040	0.0058	**0.0045**	0.0018	0.0030	0.0034	**0.0027**
Total cysteinylglycine	**0.50****	1.28	1.15	1.28	**1.23**	0.513	0.731	0.610	**0.618**
Total γ-glutamylcysteine	**0.68**	0.40	0.34	0.35	**0.366**	0.206	0.218	0.320	**0.248**
Total glutathione	**0.50**	3.89	2.80	2.81	**3.17**	1.58	0.58	2.55	**1.57**
Cysteamine	**0.54****	0.0736	0.0631	0.0749	**0.070**	0.030	0.043	0.042	**0.038**
Hypotaurine	**0.72**	0.51	0.47	0.41	**0.47**	0.22	0.31	0.49	**0.34**
Taurine	**1.16**	376	348	403	**376**	451	323	538	**437**
C-1 related metabolites									
AICA-riboside	**22.31***	0.0028	0.0030	0.0018	**0.0025**	0.060	0.040	0.068	**0.056**
SAICA-riboside	**11.50***	0.0035	0.0030	0.0034	**0.0033**	0.041	0.027	0.045	**0.038**
Glycine	**1.08**	37.8	36.9	41.7	**38.8**	42.1	29.9	53.4	**41.8**
Serine	**0.91**	2.89	2.54	2.69	**2.71**	2.29	2.14	2.96	**2.47**
Other substrates									
Dimethylglycine	**0.57**	0.035	0.098	0.053	**0.062**	0.025	0.043	0.038	**0.035**
Betaine	**0.78**	0.230	0.532	0.376	**0.380**	0.258	0.231	0.396	**0.295**
Choline	**0.75**	9.77	8.77	10.54	**9.69**	5.51	7.62	8.59	**7.24**
Sarcosine	**1.42**	0.049	0.043	0.032	**0.041**	0.043	0.063	0.070	**0.059**

* $p < 0.05$.
** $p < 0.01$.

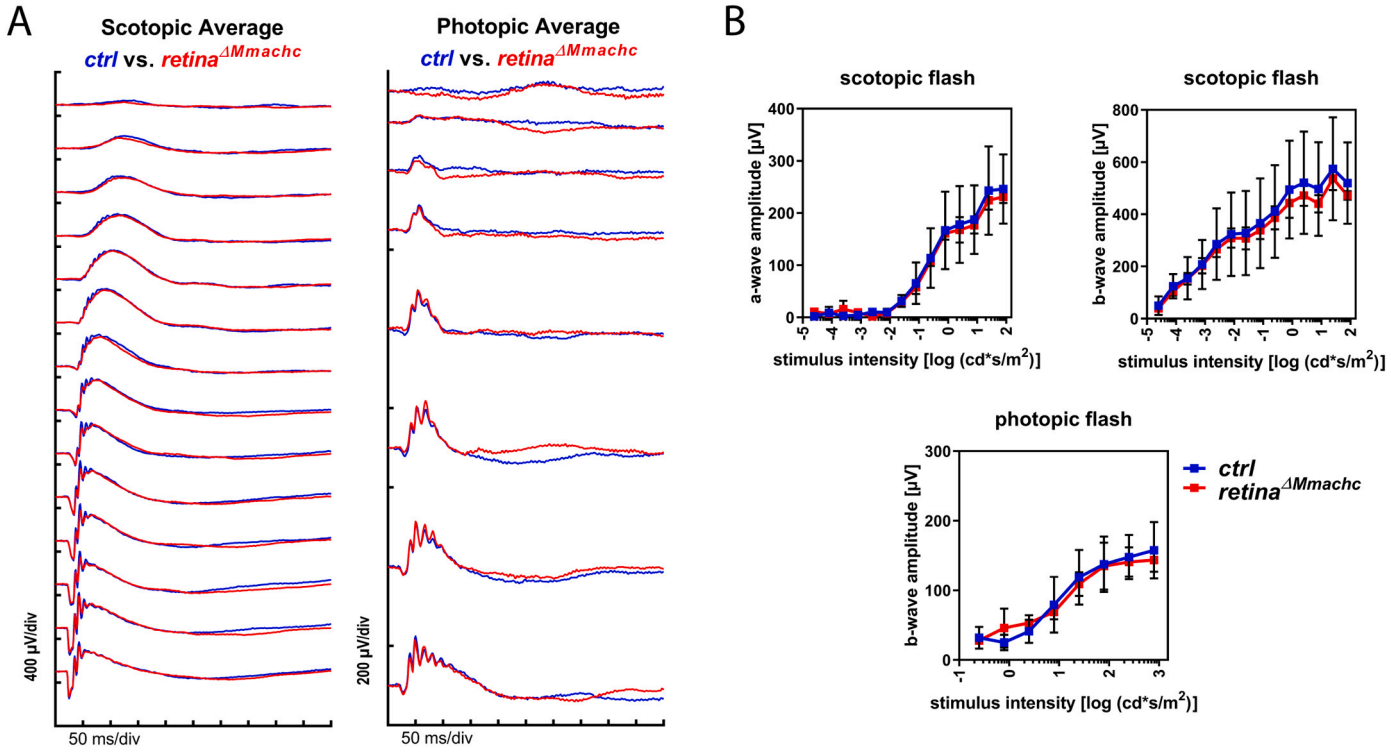

Fig. 3. Retinal function in retina$^{\Delta Mmachc}$ mice. ERG recorded in retina$^{\Delta Mmachc}$ (red, n = 4) and *Mmachc*$^{flox/flox}$ (ctrl, blue, n = 3) mice at 24 weeks of age. A) Shown are overlays of the averaged responses to light stimuli of increasing intensity (from top to bottom) recorded under scotopic (left) and photopic (right) conditions. B) Scotopic a- and b-wave (upper) and photopic b-wave (bottom) amplitudes (y-axis) plotted against light intensities (x-axis). Shown are means ± SD of both eyes of all animals per group. Statistical analysis was performed using two-way ANOVA and Sidak's correction.

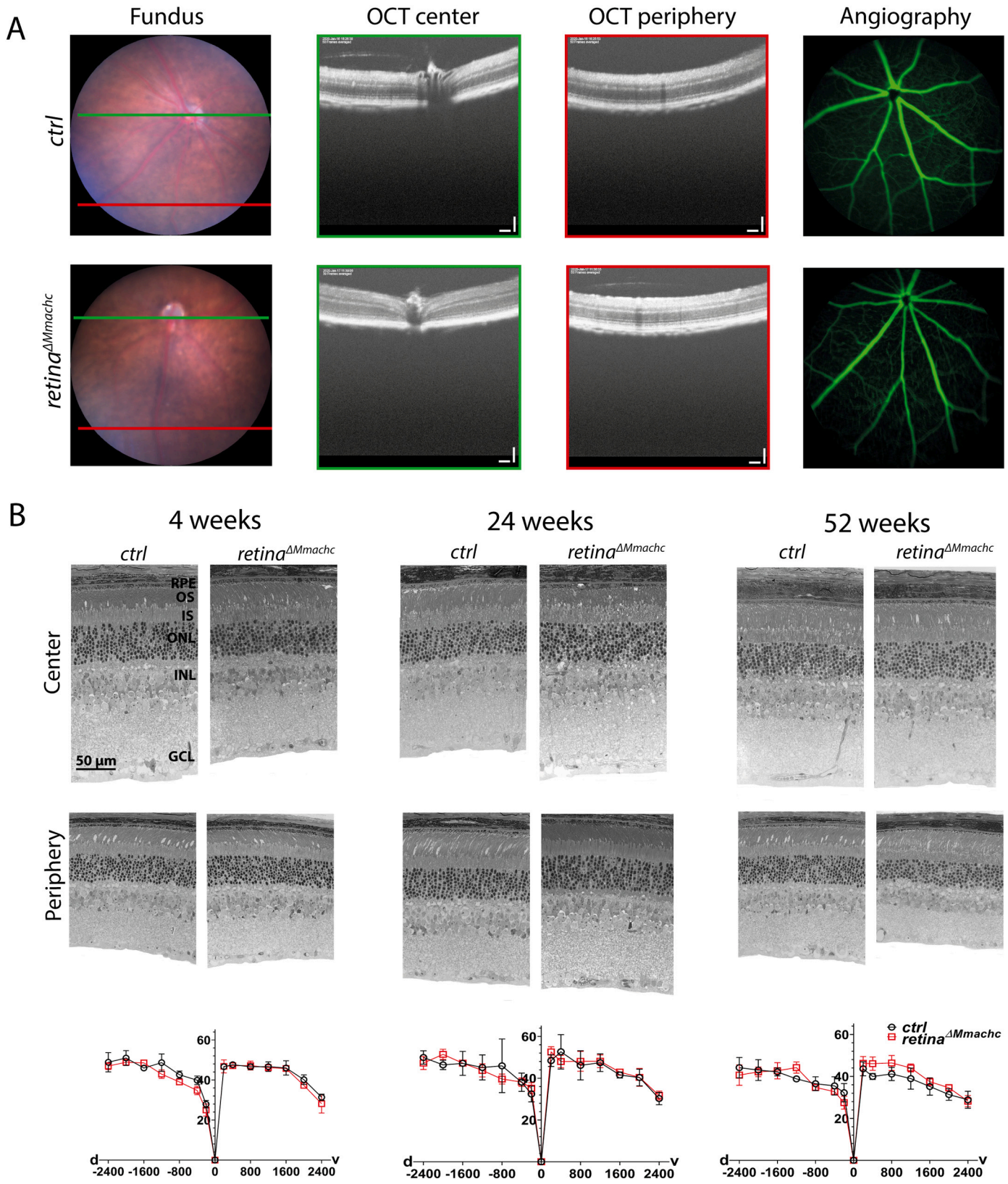

Fig. 4. Retinal morphology of retina$^{\Delta Mmachc}$ mice. A) Representative fundus images (left panels), OCT scans (middle panels), and fluorescence angiography images (right panels) of *Mmachc*$^{flox/flox}$ (ctrl) and retina$^{\Delta Mmachc}$ mice at 24 weeks of age. Colored lines indicate OCT scan position in the central (green) and more peripheral retina (red). Scale bars: 100 µm. B) Morphology of the central (top panels) and peripheral (bottom panels) retina of *Mmachc*$^{flox/flox}$ (ctrl) and retina$^{\Delta Mmachc}$ mice at 4, 24, and 52 weeks of age. Scale bar as indicated. RPE: retinal pigment epithelium, OS: outer segments, IS: inner segments, ONL: outer nuclear layer, INL: inner nuclear layer, GCL: ganglion cell layer. Bottom row panels: ONL thickness (y-axis in µm) in indicated strains was determined at 4, 24 and 52 weeks of age at 14 positions (x-axis in µm) ventral (v) and dorsal (d) of the optic nerve head (0) and presented as spidergrams. Shown are means ± SD of n = 3.

3.6. Integrity and distribution of retinal cells is normal in retina$^{\Delta Mmachc}$ mice

Finally, we examined whether the distribution of individual cell types in the peripheral nasal retina was altered. Using immunofluorescence staining, we found the distribution of cone (cone arrestin, ARR3, alias CAR), rod (rhodopsin, RHO), horizontal (calbindin-1, CALB1), amacrine (calbindin-2, CALB2), bipolar (visual system homeobox 2, VSX2 alias CHX10), and ganglion (POU domain, class 4, transcription factor, PO4F1, alias BRN3A) cell markers to be similar in 12-week-old control and retina$^{\Delta Mmachc}$ mice (Fig. 5A). In addition, similar expression levels of retinal marker genes as well as glial fibrillary acidic protein (*Gfap*), an indicator of retinal stress and activation of Müller glia cells, were found in whole retinal samples of control and retina$^{\Delta Mmachc}$ mice (Fig. 5B).

We conclude that deletion of *Mmachc* from retinal cells increased local concentrations of several metabolites, including MMA but did not lead to defects in retinal tissue integrity or retinal function in mice.

4. Discussion

The ocular phenotype in cblC patients is variable and includes degeneration of the central retina, bull's eye, optic nerve and chorioretinal atrophies, vessel attenuation, nystagmus, strabismus, and colobomas [10–13,15,16]. Although early treatment with OHCbl and betaine usually results in a substantial systemic reduction of MMA and tHcy levels and alleviates many clinical symptoms, including stabilization or amelioration of some neurologic symptoms [3], it appears to have little or no effect on the ocular phenotypes that persist despite treatment, often leading to legal blindness [12]. The reason for this lack of treatment success is unknown, as is the mechanistic basis for the ocular phenotypes. One possibility is that systemic metabolites such as MMA or Hcy cross the blood-retina-barrier causing cell damage and loss of function in retinal neurons. However, patients with isolated methylmalonic aciduria, including cblA, cblB, and mut-type deficiency (resulting from mutation of *MMAA*, *MMAB* and *MMUT*, respectively) are known to have highly elevated MMA levels but do not display the same eye phenotypes as cblC patients [11,30,32]. Furthermore, patients suffering from CBS deficiency (classical homocystinuria) are reported to have much higher Hcy levels than cblC patients, but again do not display the same eye phenotypes [13,37]. Together, this suggests that elevated systemic levels of Hcy or MMA individually are not the cause of the ocular phenotype in cblC patients, although a synergic effect cannot be excluded. Another possible explanation for the ocular phenotype is that MMACHC has a local metabolic or other as yet unknown function in the retina that is needed for sustaining retinal integrity and function. Since such a potential function may not be directly connected to vitamin B_{12} metabolism, it might not be possible to rescue it by systemic OHCbl supplementation.

The ocular consequences of reduced or absent MMACHC function has so far been difficult to investigate as no retinal tissue is available from patients, and systemic deletion of *Mmachc* is embryonically lethal in mouse models [39,41]. In contrast to mice, zebrafish with a homozygous *Mmachc* knockout survive up to 35 days post fertilization and can be used to test some aspects of Cbl deficiency [40]. Zebrafish lacking *Mmachc* activity accumulate MMA and other cblC related metabolites, display retinopathies, optic nerve thinning, a decreased ONL thickness, shortened photoreceptor outer segments, and loss of photoreceptors at 28 days post-fertilization, but not at earlier time points [40]. Still, these data do not allow discrimination between a systemic or a local cause of the ocular disease. To investigate the possibility that functional MMACHC protein is required locally in retinal cells, we generated and studied a mouse model that lacks *Mmachc* in cells of the peripheral but not central retina. Thus, each retina has its own intrinsic control region that can be used to evaluate the potential effects of the knockout.

Mmachc was found to be expressed in the retina and RPE of mouse (and human) eyes, and retina$^{\Delta Mmachc}$ mice accumulated MMA (a marker of disturbed adenosylcobalamin-dependent methylmalonyl-CoA mutase) and purine intermediates (markers of disturbed methylcobalamin-dependent one carbon metabolism and methionine synthase), which indicated a knocked down function of MMACHC in ocular cells. However, no ocular phenotype evolved in retina$^{\Delta Mmachc}$ mice. This finding is surprising as MMACHC has an essential function in Cbl processing required for odd-chain fatty acid and branched-chain amino acid metabolism [55–57] as well as methionine and SAM synthesis [58–60]. Although cells that underwent recombination may still express a shorter mRNA at reduced levels, it seems unlikely that a functional protein was generated. The mRNA lacking exons 3 and 4 retained only the sequence coding for the N-terminal 91 amino acids, while the sequence for the remaining 188 amino acids of wild type MMACHC is out of frame and removed from the RNA. This mimics the situation in patients carrying the c.271dupA variant that leads to a change of amino acid residue 91 from arginine to lysine and to a frameshift with a premature STOP 14 codons downstream (p. Arg91Lysfs*14), and means that a potentially expressed truncated MMACHC protein would lack key components required for Cbl binding and enzymatic function [5,33,52,53].

Even though no phenotype evolved, retinas of retina$^{\Delta Mmachc}$ mice showed significantly altered metabolite levels that are relevant for cblC disease. MMA was increased by a factor of 5.6, suggesting an impairment of the AdoCbl-dependent MMUT. Since Hcy levels tended to be slightly increased and Met to be slightly decreased, a tendency of a reduced Met/Hcy ratio was noted in retina$^{\Delta Mmachc}$ mice (Table 1). Although significance was not reached, probably owed to the analysis of whole retinas that included the central areas where *Mmachc* was not deleted, this data might indicate that remethylation of Hcy to Met could be affected. It has emerged that patients with cblG (methionine synthase deficiency) and cblE (methionine synthase reductase deficiency) defects can show similar ocular findings as those with cblC defects, suggesting that a local impairment of homocysteine remethylation could contribute to eye disease development [3,13]. Interestingly, the dephosphorylated *de novo* purine synthesis intermediates, AICA-riboside and SAICA-riboside, were strongly increased (22.3-fold and 11.5-fold, respectively) in retina$^{\Delta Mmachc}$ mice. Since these intermediates are immediately upstream of the AICA-riboside transformylase catalyzed 10-formyl-tetrahydrofolate-dependent reaction, their elevation may represent indirect evidence of a methyl folate trap [61–63]. A publication by Sanderson et al. [64] described that purines have the ability to modulate the physiological processes of retinal neurons, astrocytes, Müller cells, lens, trabecular meshwork, cornea, lacrimal gland and RPE *via* ATP release mechanisms, receptor interactions and signaling pathways. In addition, several publications suggest that AICA-riboside is neuroprotective and anti-inflammatory in the retina through its activation of the AMPK pathway [34,65]. It may therefore be worth investigating further the impact of these elevated purine synthesis related metabolites on cell signaling/function. Additionally, in accordance with a previous report which found decreased total and reduced GSH in lymphocytes from cblC patients [8], we also observed decreased retinal concentration of total GSH, its precursor gamma-glutamylcysteine and its degradation product cysteinylglycine in our mouse model. These data indicate that the putatively impaired antioxidant defense may not play a role in the ocular phenotype of the cblC disease in these mice. The lack of a pathological phenotype in retina$^{\Delta Mmachc}$ mice may also be surprising in light of the severe eye phenotype in mouse embryos with a full-body *Mmachc* knockout [41]. However, this eye phenotype may be caused by developmental deficits originating much earlier than at E10.5, the time point when the Pax6-Cre mice start to express Cre [42] to inactivate the *Mmachc* gene in retinal progenitor cells in our model. Thus, our data suggest that local *Mmachc* might be dispensable for retinal development, maintenance and function, at least in the mouse. Despite the differences between human and mouse retinas, this might indicate that the ocular phenotype in cblC patients carrying mutations such as c.271dupA in

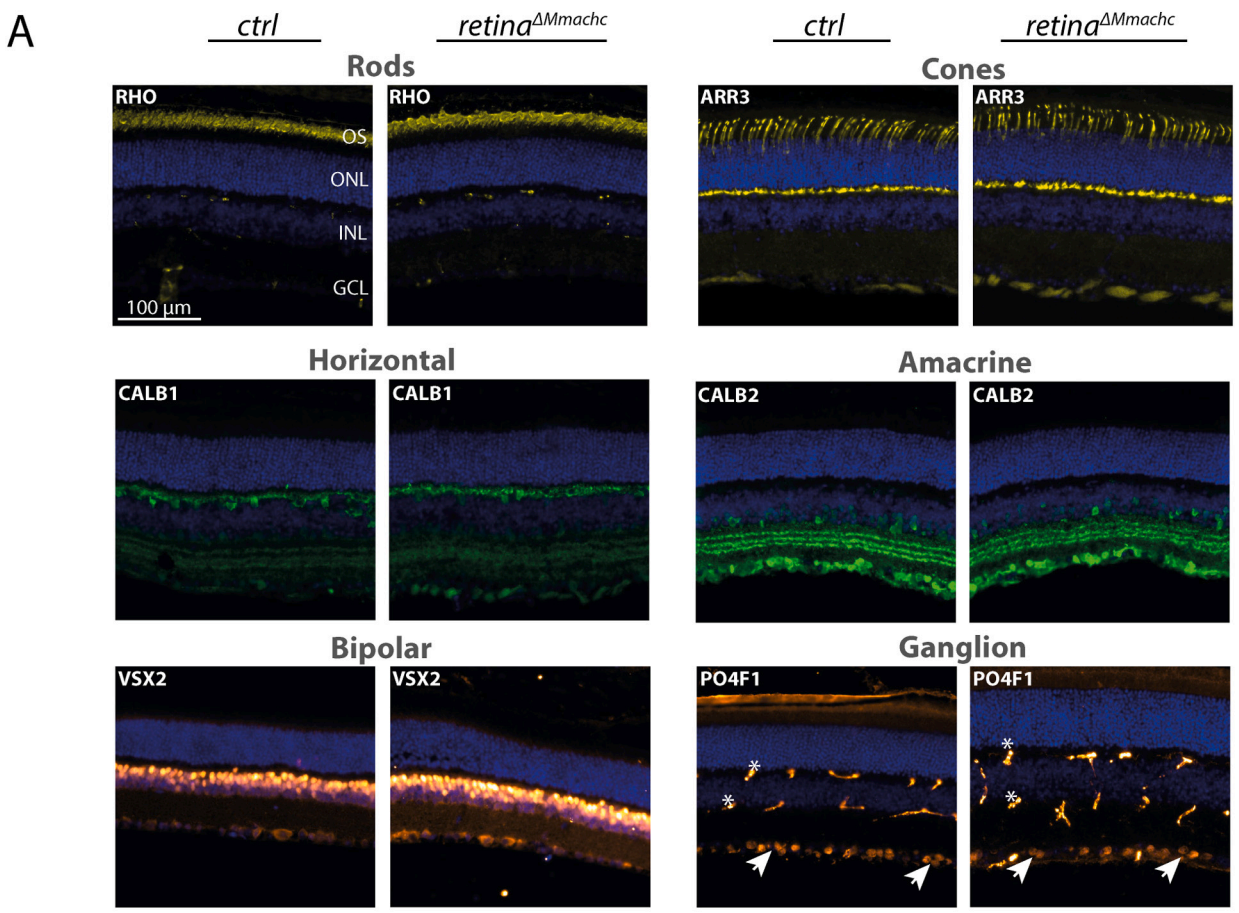

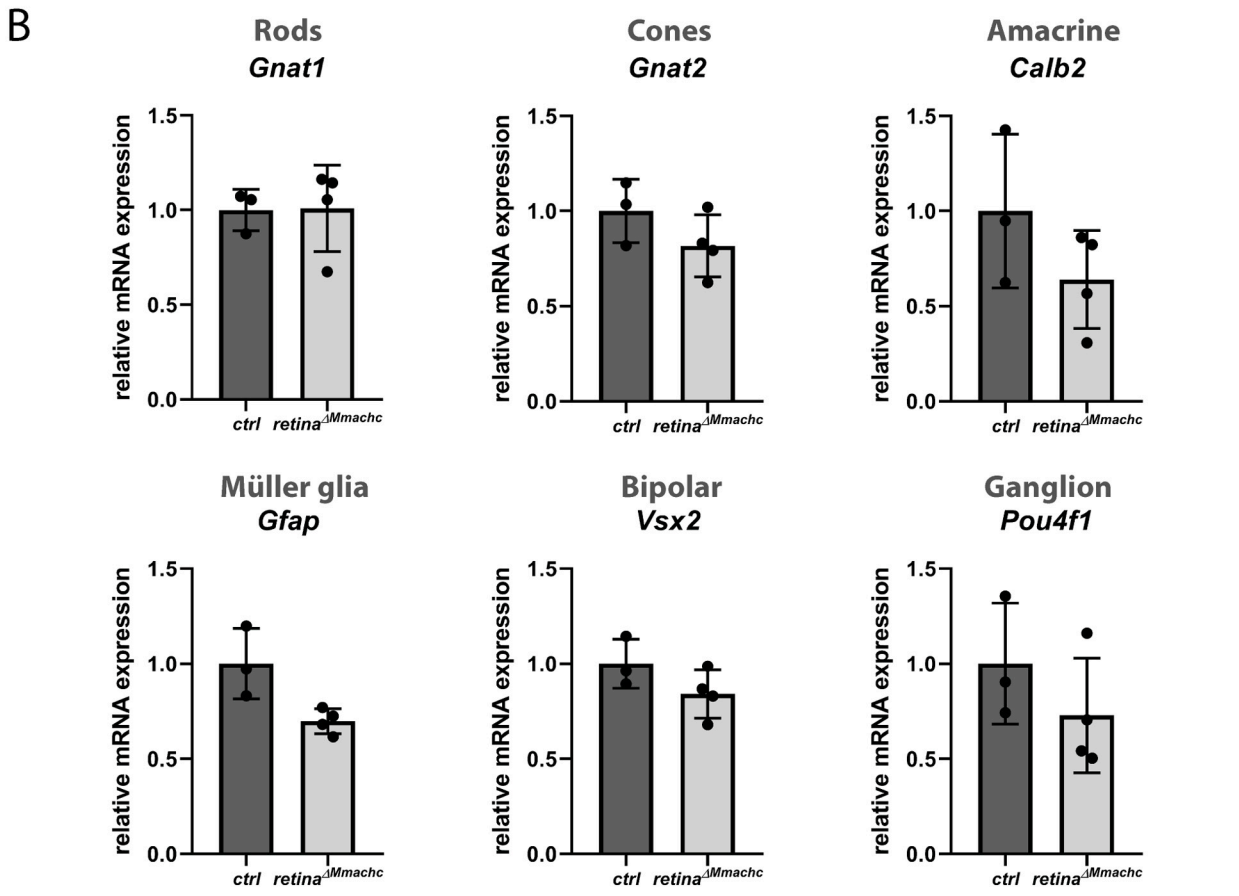

(caption on next page)

Fig. 5. Expression of markers of retinal cells in retina$^{\Delta Mmachc}$ mice. A) Immunofluorescence micrographs of cryosections of the peripheral retina from 12-week-old *Mmachc*$^{flox/flox}$ (ctrl, left panels) and retina$^{\Delta Mmachc}$ mice (right panels) showing immunolabeled rods (RHO), cones (ARR3), horizontal cells (CALB1), amacrine cells (CALB2), bipolar cells (VSX2), and ganglion cells (PO4F1). Shown are images from the peripheral retina (area between 1600 and 2400 μm from the optic nerve head). DAPI: blue. Scale bar as indicated. OS: outer segments, ONL: outer nuclear layer, INL: inner nuclear layer, GCL: ganglion cell layer. B) Relative mRNA expression levels of retinal cell markers in 8-week-old *Mmach*$^{flox/flox}$ (ctrl, $n = 3$) and retina$^{\Delta Mmachc}$ mice ($n = 4$). RNA levels of rod- (rod transducin; *Gnat1*), cone- (cone transducin; *Gnat 2*), amacrine cell- (calbindin-2; *Calb2*), astrocytes and glia cell- (glial fibrillary acidic protein; *Gfap*), bipolar cell- (visual system homeobox 2; *Vsx2*) and ganglion cell- (POU class 4 homeobox 1; *Pou4f1*) specific genes were tested by qPCR in retinal tissue. Transcript levels of controls were set to 1. Shown are individual data points, means ± SD, n = 3. Statistical analysis was performed using unpaired *t*-test with Welch's correction.

MMACHC may be inflicted through systemic effects, even though a local role cannot completely be excluded.

The lack of a peripheral retinal phenotype in our model may alternatively be explained by the existence of wild type cells in the vicinity of retinal cells lacking *Mmachc*. Not only cells of the central retina, but also those of the lens, cornea, and RPE lack expression of *Pax6-Cre* [42] and thus express wild-type MMACHC protein. These cells might support the knockout cells by supplying sufficient essential metabolites needed for cell survival and function. A study in pigs [66] has indeed shown that metabolites can be exchanged even between organs *via* the bloodstream. Possible candidate cell types for such an auxiliary function in the eye might be endothelial cells that nourish the cells of the inner retina, and cells of the RPE that form the outer blood-retina-barrier and play an essential role in supporting photoreceptors in the outer retina by providing nutrients and metabolites that originate from the choroidal circulation [67,68]. We will test this hypothesis by inactivating *Mmachc* specifically in the RPE of retina$^{\Delta Mmachc}$ and *Mmachc*$^{flox/flox}$ mice.

Since mice lack a macula, the region most strongly affected in cblC patients [12,13,15,16,69], data from mouse models have to be interpreted with caution. However, in the absence of animal models that completely reflect the human retinal architecture and function (only humans and non-human primates possess a macula), data from mice and other models such as zebrafish [70] often provide a first step in the investigation of ocular consequences of specific gene mutations. Nevertheless, since human and the mouse retina are rod dominated with a rod to cone distribution of 95% to 5% (human) and 97% to 3% (mouse) [71–73] while retinal layering, the types of neurons in the retina, the physiology of vision including scotopic and photopic vision, regenerative pathways of the visual chromophore as well as retinal and choroidal vasculature are largely comparable between the two [74–77], mice have played an important role in the study of retinal degenerative diseases. Here, we chose to use *Pax6-Cre* deleter mice to inactivate *Mmachc* from retinal neurons. Although this spares cells from the central retina, a large area of an estimated 70% is affected by the deletion [43,51]. This leads to retinas with an intrinsic control region (center) that facilitates interpretations (see *e.g.* [51]). Even though our mouse model has limitations, our data strongly argue that individual retinal neurons lacking *Mmachc* expression can survive in the context of the retinal tissue in mice. Should retinal symptoms be caused by systemic rather than local effects, as our current data suggest, it remains to be explained why treatments, including systemic supplementation with Cbl, betaine and potentially folinic acid, improve many symptoms including some neurologic problems, but do not rescue retinal phenotypes. It might be possible that they cannot reverse pre-existing alterations in the delicate retinal cells, especially if the neurons have already entered a degenerative pathway. Although intriguing, this however remains speculative and requires further investigation.

CRediT authorship contribution statement

Eva Kiessling: Methodology, Formal analysis, Investigation, Writing – original draft. **Sarah Nötzli:** Investigation. **Vyara Todorova:** Formal analysis. **Merima Forny:** Methodology, Resources. **Matthias R. Baumgartner:** Conceptualization, Writing – review & editing, Funding acquisition. **Marijana Samardzija:** Supervision, Formal analysis. **Jakub Krijt:** Methodology, Formal analysis, Investigation. **Viktor Kožich:** Formal analysis, Writing – review & editing, Funding acquisition. **Christian Grimm:** Conceptualization, Writing – original draft, Supervision, Project administration, Funding acquisition. **D. Sean Froese:** Conceptualization, Writing – original draft, Supervision, Project administration, Funding acquisition.

Declaration of competing interest

The authors declare that they have no known competing financial interests or personal relationships that could have appeared to influence the work reported in this paper.

Acknowledgments

This project was supported by the Wolfermann-Nägeli Stiftung, Switzerland, and the Swiss National Science Foundation ([31003A_175779] to MRB, [310030_192505] to DSF). M.B. received financial support from the University Research Priority Program of the University of Zurich (URPP) ITINERARE - Innovative Therapies in Rare Diseases. VK and JK were in part supported by the grant GAČR 19-08786S from the Czech Science Foundation and received institutional support from the project RVO-VFN 64165. The authors thank Isabelle Meneau for the collection of the human samples, Cornelia Imsand, Adrian Urwyler, Celine Bürer, Jitka Sokolová and Tereza Vaculíková Fantlová for their excellent technical assistance.

Appendix A. Supplementary data

Supplementary data to this article can be found online at https://doi.org/10.1016/j.bbadis.2021.166201.

References

[1] D. Watkins, D.S. Rosenblatt, Lessons in biology from patients with inherited disorders of vitamin B12 and folate metabolism, Biochimie 126 (2016) 3–5, https://doi.org/10.1016/j.biochi.2016.05.001.

[2] S. Fischer, M. Huemer, M. Baumgartner, F. Deodato, D. Ballhausen, A. Boneh, A. B. Burlina, R. Cerone, P. Garcia, G. Gokcay, S. Grunewald, J. Haberle, J. Jaeken, D. Ketteridge, M. Lindner, H. Mandel, D. Martinelli, E.G. Martins, K.O. Schwab, S. C. Gruenert, B.C. Schwahn, L. Sztriha, M. Tomaske, F. Trefz, L. Vilarinho, D. S. Rosenblatt, B. Fowler, C. Dionisi-Vici, Clinical presentation and outcome in a series of 88 patients with the cblC defect, J. Inherit. Metab. Dis. 37 (2014) 831–840, https://doi.org/10.1007/s10545-014-9687-6.

[3] M. Huemer, D. Diodato, B. Schwahn, M. Schiff, A. Bandeira, J.F. Benoist, A. Burlina, R. Cerone, M.L. Couce, A. Garcia-Cazorla, G. la Marca, E. Pasquini, L. Vilarinho, J.D. Weisfeld-Adams, V. Kozich, H. Blom, M.R. Baumgartner, C. Dionisi-Vici, Guidelines for diagnosis and management of the cobalamin-related remethylation disorders cblC, cblD, cblE, cblF, cblG, cblJ and MTHFR deficiency, J. Inherit. Metab. Dis. 40 (2017) 21–48, https://doi.org/10.1007/s10545-016-9991-4.

[4] J.D. Weisfeld-Adams, H.A. Bender, A. Miley-Akerstedt, T. Frempong, N.L. Schrager, K. Patel, T.P. Naidich, V. Stein, J. Spat, S. Towns, M.P. Wasserstein, I. Peter, Y. Frank, G.A. Diaz, Neurologic and neurodevelopmental phenotypes in young children with early-treated combined methylmalonic acidemia and homocystinuria, cobalamin C type, Mol. Genet. Metab. 110 (2013) 241–247, https://doi.org/10.1016/j.ymgme.2013.07.018.

[5] J.P. Lerner-Ellis, N. Anastasio, J. Liu, D. Coelho, T. Suormala, M. Stucki, A. D. Loewy, S. Gurd, E. Grundberg, C.F. Morel, D. Watkins, M.R. Baumgartner, T. Pastinen, D.S. Rosenblatt, B. Fowler, Spectrum of mutations in MMACHC, allelic expression, and evidence for genotype-phenotype correlations, Hum. Mutat. 30 (2009) 1072–1081, https://doi.org/10.1002/humu.21001.

[6] E.R. Baumgartner, H. Wick, J.C. Linnell, G.E. Gaull, C. Bachmann, B. Steinmann, Congenital defect in intracellular cobalamin metabolism resulting in homocystinuria and methylmalonic aciduria. II. Biochemical investigations, Helv. Paediatr. Acta 34 (1979) 483–496.

[7] M. Caterino, A. Pastore, M.G. Strozziero, G. Di Giovamberardino, E. Imperlini, E. Scolamiero, L. Ingenito, S. Boenzi, F. Ceravolo, D. Martinelli, C. Dionisi-Vici, M. Ruoppolo, The proteome of cblC defect: in vivo elucidation of altered cellular pathways in humans, J. Inherit. Metab. Dis. 38 (2015) 969–979, https://doi.org/10.1007/s10545-014-9806-4.

[8] A. Pastore, D. Martinelli, F. Piemonte, G. Tozzi, S. Boenzi, G. Di Giovamberardino, S. Petrillo, E. Bertini, C. Dionisi-Vici, Glutathione metabolism in cobalamin deficiency type C (cblC), J. Inherit. Metab. Dis. 37 (2014) 125–129, https://doi.org/10.1007/s10545-013-9605-3.

[9] R.C. Ahrens-Nicklas, A.M. Whitaker, P. Kaplan, S. Cuddapah, J. Burfield, J. Blair, L. Brochi, M. Yudkoff, C. Ficicioglu, Efficacy of early treatment in patients with cobalamin C disease identified by newborn screening: a 16-year experience, Genet. Med. 19 (2017) 926–935, https://doi.org/10.1038/gim.2016.214.

[10] T.S. Aleman, F. Brodie, C. Garvin, D.Y. Gewaily, C.H. Ficicioglu, M.D. Mills, B. J. Forbes, A.M. Maguire, S.L. Davidson, Retinal structure in cobalamin C disease: mechanistic and therapeutic implications, Ophthalmic Genet. 36 (2015) 339–348, https://doi.org/10.3109/13816810.2014.885059.

[11] G.M. Bacci, M.A. Donati, E. Pasquini, F. Munier, C. Cavicchi, A. Morrone, A. Sodi, V. Murro, N. Garcia Segarra, C. Defilippi, L. Bussolin, R. Caputo, Optical coherence tomography morphology and evolution in cblC disease-related maculopathy in a case series of very young patients, Acta Ophthalmol. 95 (2017) e776–e782, https://doi.org/10.1111/aos.13441.

[12] L. Bonafede, C.H. Ficicioglu, L. Serrano, G. Han, J.I. Morgan, M.D. Mills, B. J. Forbes, S.L. Davidson, G. Binenbaum, P.B. Kaplan, C.W. Nichols, P. Verloo, B. P. Leroy, A.M. Maguire, T.S. Aleman, Cobalamin C deficiency shows a rapidly progressing maculopathy with severe photoreceptor and ganglion cell loss, Invest. Ophthalmol. Vis. Sci. 56 (2015) 7875–7887, https://doi.org/10.1167/iovs.15-17857.

[13] B.P. Brooks, A.H. Thompson, J.L. Sloan, I. Manoli, N. Carrillo-Carrasco, W.M. Zein, C.P. Venditti, Ophthalmic manifestations and long-term visual outcomes in patients with cobalamin C deficiency, Ophthalmology 123 (2016) 571–582, https://doi.org/10.1016/j.ophtha.2015.10.041.

[14] N. Carrillo-Carrasco, C.P. Venditti, Combined methylmalonic acidemia and homocystinuria, cblC type. II. Complications, pathophysiology, and outcomes, J. Inherit. Metab. Dis. 35 (2012) 103–114, https://doi.org/10.1007/s10545-011-9365-x.

[15] L.R. Fuchs, M. Robert, I. Ingster-Moati, L. Couette, J.L. Dufier, P. de Lonlay, S. E. Brodie, Ocular manifestations of cobalamin C type methylmalonic aciduria with homocystinuria, J. AAPOS 16 (2012) 370–375, https://doi.org/10.1016/j.jaapos.2012.02.019.

[16] C. Gerth, C.F. Morel, A. Feigenbaum, A.V. Levin, Ocular phenotype in patients with methylmalonic aciduria and homocystinuria, cobalamin C type, J. AAPOS 12 (2008) 591–596, https://doi.org/10.1016/j.jaapos.2008.06.008.

[17] R. Gizicki, M.C. Robert, L. Gomez-Lopez, J. Orquin, J.C. Decarie, G.A. Mitchell, M. S. Roy, L.H. Ospina, Long-term visual outcome of methylmalonic aciduria and homocystinuria, cobalamin C type, Ophthalmology 121 (2014) 381–386, https://doi.org/10.1016/j.ophtha.2013.08.034.

[18] D.S. Rosenblatt, A.L. Aspler, M.I. Shevell, B.A. Pletcher, W.A. Fenton, M. R. Seashore, Clinical heterogeneity and prognosis in combined methylmalonic aciduria and homocystinuria (cblC), J. Inherit. Metab. Dis. 20 (1997) 528–538, https://doi.org/10.1023/a:1005353530303.

[19] J.D. Weisfeld-Adams, M.A. Morrissey, B.M. Kirmse, B.R. Salveson, M. P. Wasserstein, P.J. McGuire, S. Sunny, J.L. Cohen-Pfeffer, C. Yu, M. Caggana, G. A. Diaz, Newborn screening and early biochemical follow-up in combined methylmalonic aciduria and homocystinuria, cblC type, and utility of methionine as a secondary screening analyte, Mol. Genet. Metab. 99 (2010) 116–123, https://doi.org/10.1016/j.ymgme.2009.09.008.

[20] N. Carrillo-Carrasco, R.J. Chandler, C.P. Venditti, Combined methylmalonic acidemia and homocystinuria, cblC type. I. Clinical presentations, diagnosis and management, J. Inherit. Metab. Dis. 35 (2012) 91–102, https://doi.org/10.1007/s10545-011-9364-y.

[21] E. Andres, N.H. Loukili, E. Noel, G. Kaltenbach, M.B. Abdelgheni, A.E. Perrin, M. Noblet-Dick, F. Maloisel, J.L. Schlienger, J.F. Blickle, Vitamin B12 (cobalamin) deficiency in elderly patients, CMAJ 171 (2004) 251–259, https://doi.org/10.1503/cmaj.1031155.

[22] M.J. Nielsen, M.R. Rasmussen, C.B. Andersen, E. Nexo, S.K. Moestrup, Vitamin B12 transport from food to the body's cells—a sophisticated, multistep pathway, Nat. Rev. Gastroenterol. Hepatol. 9 (2012) 345–354, https://doi.org/10.1038/nrgastro.2012.76.

[23] S.M. Tanner, A.C. Sturm, E.C. Baack, S. Liyanarachchi, A. de la Chapelle, Inherited cobalamin malabsorption. Mutations in three genes reveal functional and ethnic patterns, Orphanet. J. Rare Dis. 7 (2012) 56, https://doi.org/10.1186/1750-1172-7-56.

[24] E.V. Quadros, J.M. Sequeira, Cellular uptake of cobalamin: transcobalamin and the TCblR/CD320 receptor, Biochimie 95 (2013) 1008–1018, https://doi.org/10.1016/j.biochi.2013.02.004.

[25] B. Kräutler, Vitamin B12: chemistry and biochemistry, Biochem. Soc. Trans. 33 (2005) 806–810, https://doi.org/10.1042/BST0330806 (%J Biochemical Society Transactions).

[26] D.S. Froese, J. Kopec, F. Fitzpatrick, M. Schuller, T.J. McCorvie, R. Chalk, T. Plessl, V. Fettelschoss, B. Fowler, M.R. Baumgartner, W.W. Yue, Structural insights into the MMACHC-MMADHC protein complex involved in vitamin B12 trafficking, J. Biol. Chem. 290 (2015) 29167–29177, https://doi.org/10.1074/jbc.M115.683268.

[27] J. Kim, C. Gherasim, R. Banerjee, Decyanation of vitamin B12 by a trafficking chaperone, Proc. Natl. Acad. Sci. U. S. A. 105 (2008) 14551–14554, https://doi.org/10.1073/pnas.0805989105.

[28] C.F. Morel, J.P. Lerner-Ellis, D.S. Rosenblatt, Combined methylmalonic aciduria and homocystinuria (cblC): phenotype-genotype correlations and ethnic-specific observations, Mol. Genet. Metab. 88 (2006) 315–321, https://doi.org/10.1016/j.ymgme.2006.04.001.

[29] J.L. Sloan, N. Carrillo, D. Adams, C.P. Venditti, Disorders of intracellular cobalamin metabolism, Hum. Mol. Genet. (2020) 2109–2123, https://doi.org/10.1093/hmg/ddaa044.

[30] D. Watkins, D.S. Rosenblatt, Inherited disorders of folate and cobalamin transport and metabolism, in: D.L. Valle, S. Antonarakis, A. Ballabio, A.L. Beaudet, G. A. Mitchell (Eds.), The Online Metabolic and Molecular Bases of Inherited Disease, McGraw-Hill Education, New York, NY, 2019.

[31] B. Fowler, J.V. Leonard, M.R. Baumgartner, Causes of and diagnostic approach to methylmalonic acidurias, J. Inherit. Metab. Dis. 31 (2008) 350–360, https://doi.org/10.1007/s10545-008-0839-4.

[32] D.S. Froese, R.A. Gravel, Genetic disorders of vitamin B(1)(2) metabolism: eight complementation groups—eight genes, Expert Rev. Mol. Med. 12 (2010), e37, https://doi.org/10.1017/S1462399410001651.

[33] J.P. Lerner-Ellis, J.C. Tirone, P.D. Pawelek, C. Dore, J.L. Atkinson, D. Watkins, C. F. Morel, T.M. Fujiwara, E. Moras, A.R. Hosack, G.V. Dunbar, H. Antonicka, V. Forgetta, C.M. Dobson, D. Leclerc, R.A. Gravel, E.A. Shoubridge, J.W. Coulton, P. Lepage, J.M. Rommens, K. Morgan, D.S. Rosenblatt, Identification of the gene responsible for methylmalonic aciduria and homocystinuria, cblC type, Nat. Genet. 38 (2006) 93–100, https://doi.org/10.1038/ng1683.

[34] M. Kamoshita, K. Fujinami, E. Toda, K. Tsubota, Y. Ozawa, Neuroprotective effect of activated 5′-adenosine monophosphate-activated protein kinase on cone system function during retinal inflammation, BMC Neurosci. 17 (2016) 32, https://doi.org/10.1186/s12868-016-0268-5.

[35] C.A. Ku, J.K. Ng, D.J. Karr, L. Reznick, C.O. Harding, R.G. Weleber, M.E. Pennesi, Spectrum of ocular manifestations in cobalamin C and cobalamin A types of methylmalonic acidemia, Ophthalmic Genet. 37 (2016) 404–414, https://doi.org/10.3109/13816810.2015.1121500.

[36] T. Suormala, M.R. Baumgartner, D. Coelho, P. Zavadakova, V. Kozich, H.G. Koch, M. Berghauser, J.E. Wraith, A. Burlina, A. Sewell, J. Herwig, B. Fowler, The cblD defect causes either isolated or combined deficiency of methylcobalamin and adenosylcobalamin synthesis, J. Biol. Chem. 279 (2004) 42742–42749, https://doi.org/10.1074/jbc.M407733200.

[37] L.A. Kluijtmans, G.H. Boers, J.P. Kraus, L.P. van den Heuvel, J.R. Cruysberg, F. J. Trijbels, H.J. Blom, The molecular basis of cystathionine beta-synthase deficiency in Dutch patients with homocystinuria: effect of CBS genotype on biochemical and clinical phenotype and on response to treatment, Am. J. Hum. Genet. 65 (1999) 59–67, https://doi.org/10.1086/302439.

[38] A. Tawfik, Y.A. Samra, N.M. Elsherbiny, M. Al-Shabrawey, Implication of hyperhomocysteinemia in Blood Retinal Barrier (BRB) dysfunction, Biomolecules 10 (2020), https://doi.org/10.3390/biom10081119.

[39] M.A. Moreno-Garcia, M. Pupavac, D.S. Rosenblatt, M.L. Tremblay, L.A. Jerome-Majewska, The Mmachc gene is required for pre-implantation embryogenesis in the mouse, Mol. Genet. Metab. 112 (2014) 198–204, https://doi.org/10.1016/j.ymgme.2014.05.002.

[40] J.L. Sloan, N.P. Achilly, M.L. Arnold, J.L. Catlett, T. Blake, K. Bishop, M. Jones, U. Harper, M.A. English, S. Anderson, N.S. Trivedi, A. Elkahloun, V. Hoffmann, B. P. Brooks, R. Sood, C.P. Venditti, The vitamin B12 processing enzyme, mmachc, is essential for zebrafish survival, growth and retinal morphology, Hum. Mol. Genet. (2020), https://doi.org/10.1093/hmg/ddaa044.

[41] T. Chern, A. Achilleos, X. Tong, C.W. Hsu, L. Wong, R.A. Poche, Mouse models to study the pathophysiology of combined methylmalonic acidemia and homocystinuria, cblC type, Dev. Biol. (2020), https://doi.org/10.1016/j.ydbio.2020.09.005.

[42] T. Marquardt, R. Ashery-Padan, N. Andrejewski, R. Scardigli, F. Guillemot, P. Gruss, Pax6 is required for the multipotent state of retinal progenitor cells, Cell 105 (2001) 43–55, https://doi.org/10.1016/s0092-8674(01)00295-1.

[43] C. Caprara, M. Thiersch, C. Lange, S. Joly, M. Samardzija, C. Grimm, HIF1A is essential for the development of the intermediate plexus of the retinal vasculature, Invest. Ophthalmol. Vis. Sci. 52 (2011) 2109–2117, https://doi.org/10.1167/iovs.10-6222.

[44] K.J. Livak, T.D. Schmittgen, Analysis of relative gene expression data using real-time quantitative PCR and the 2(−delta delta C(T)) method, Methods 25 (2001) 402–408, https://doi.org/10.1006/meth.2001.1262.

[45] J. Krijt, A. Dutá, V. Kožich, Determination of S-adenosylmethionine and S-adenosylhomocysteine by LC–MS/MS and evaluation of their stability in mice tissues, J. Chromatogr. B 877 (2009) 2061–2066, https://doi.org/10.1016/j.jchromb.2009.05.039.

[46] V. Kožich, T. Ditrói, J. Sokolová, M. Křížková, J. Krijt, P. Ješina, P. Nagy, Metabolism of sulfur compounds in homocystinurias, Br. J. Pharmacol. 176 (2019) 594–606, https://doi.org/10.1111/bph.14523.

[47] M. Svaton, K.S. Kramarzova, V. Kanderova, A. Mancikova, P. Smisek, P. Jesina, J. Krijt, B. Stiburkova, R. Dobrovolny, J. Sokolova, V. Bakardjieva-Mihaylova, E. Vodickova, M. Rackova, J. Stuchly, T. Kalina, J. Stary, J. Trka, E. Fronkova, V. Kozich, A homozygous deletion in the SLC19A1 gene as a cause of folate-dependent recurrent megaloblastic anemia, Blood 135 (2020) 2427–2431, https://doi.org/10.1182/blood.2019003178.

[48] V. Kožich, M. Vacková, J. Krijt, Measurement of homocysteine and other aminothiols in plasma: advantages of using tris(2-carboxyethyl)phosphine as

reductant compared with tri-n-butylphosphine, Clin. Chem. 47 (2001) 1821–1828, https://doi.org/10.1093/clinchem/47.10.1821.
[49] J. Krijt, M. Vacková, V. Kožich, Measurement of homocysteine and other aminothiols in plasma: advantages of using tris(2-carboxyethyl)phosphine as reductant compared with tri-n-butylphosphine, Clin. Chem. 47 (2001) 1821–1828, https://doi.org/10.1093/clinchem/47.10.1821.
[50] S. Wang, X. Lai, Y. Deng, Y. Song, Correlation between mouse age and human age in anti-tumor research: significance and method establishment, Life Sci. 242 (2020), 117242, https://doi.org/10.1016/j.lfs.2019.117242.
[51] S.R. Heynen, I. Meneau, C. Caprara, M. Samardzija, C. Imsand, E.M. Levine, C. Grimm, CDC42 is required for tissue lamination and cell survival in the mouse retina, PLoS One 8 (2013), e53806, https://doi.org/10.1371/journal.pone.0053806.
[52] D.S. Froese, T. Krojer, X. Wu, R. Shrestha, W. Kiyani, F. von Delft, R.A. Gravel, U. Oppermann, W.W. Yue, Structure of MMACHC reveals an arginine-rich pocket and a domain-swapped dimer for its B12 processing function, Biochemistry 51 (2012) 5083–5090, https://doi.org/10.1021/bi300150y.
[53] M. Koutmos, C. Gherasim, J.L. Smith, R. Banerjee, Structural basis of multifunctionality in a vitamin B12-processing enzyme, J. Biol. Chem. 286 (2011) 29780–29787, https://doi.org/10.1074/jbc.M111.261370.
[54] J.I. Morgan, The fundus photo has met its match: optical coherence tomography and adaptive optics ophthalmoscopy are here to stay, Ophthal. Physiol. Opt. 36 (2016) 218–239, https://doi.org/10.1111/opo.12289.
[55] A. Alfares, L.D. Nunez, K. Al-Thihli, J. Mitchell, S. Melancon, N. Anastasio, K.C. Ha, J. Majewski, D.S. Rosenblatt, N. Braverman, Combined malonic and methylmalonic aciduria: exome sequencing reveals mutations in the ACSF3 gene in patients with a non-classic phenotype, J. Med. Genet. 48 (2011) 602–605, https://doi.org/10.1136/jmedgenet-2011-100230.
[56] I. Manoli, J.G. Myles, J.L. Sloan, O.A. Shchelochkov, C.P. Venditti, A critical reappraisal of dietary practices in methylmalonic acidemia raises concerns about the safety of medical foods. Part 1: isolated methylmalonic acidemias, Genet. Med. 18 (2016) 386–395, https://doi.org/10.1038/gim.2015.102.
[57] J.L. Sloan, J.J. Johnston, I. Manoli, R.J. Chandler, C. Krause, N. Carrillo-Carrasco, S.D. Chandrasekaran, J.R. Sysol, K. O'Brien, N.S. Hauser, J.C. Sapp, H.M. Dorward, M. Huizing, Group NIHISC, B.A. Barshop, S.A. Berry, P.M. James, N. L. Champaigne, P. de Lonlay, V. Valayannopoulos, M.D. Geschwind, D.K. Gavrilov, W.L. Nyhan, L.G. Biesecker, C.P. Venditti, Exome sequencing identifies ACSF3 as a cause of combined malonic and methylmalonic aciduria, Nat. Genet. 43 (2011) 883–886, https://doi.org/10.1038/ng.908.
[58] L. Brunaud, J.M. Alberto, A. Ayav, P. Gerard, F. Namour, L. Antunes, M. Braun, J. P. Bronowicki, L. Bresler, J.L. Gueant, Effects of vitamin B12 and folate deficiencies on DNA methylation and carcinogenesis in rat liver, Clin. Chem. Lab. Med. 41 (2003) 1012–1019, https://doi.org/10.1515/CCLM.2003.155.
[59] S. Fernandez-Roig, S.C. Lai, M.M. Murphy, J. Fernandez-Ballart, E.V. Quadros, Vitamin B12 deficiency in the brain leads to DNA hypomethylation in the TCblR/CD320 knockout mouse, Nutr. Metab. (Lond.) 9 (2012) 41, https://doi.org/10.1186/1743-7075-9-41.
[60] B.A. Varma, S. Bashetti, R. Vijayaraghavan, K.S. Sailesh, Folic acid, vitamin B12, and DNA methylation: an update, Asian J. Pharm. Clin. Res. 11 (2018), https://doi.org/10.22159/ajpcr.2018.v11i1.21892.
[61] V. Herbert, R. Zalusky, Interrelations of vitamin B12 and folic acid metabolism: folic acid clearance studies, J. Clin. Invest. 41 (1962) 1263–1276, https://doi.org/10.1172/JCI104589.
[62] J.M. Lopez, E.L. Outtrim, R. Fu, D.J. Sutcliffe, R.J. Torres, H.A. Jinnah, Physiological levels of folic acid reveal purine alterations in Lesch-Nyhan disease, Proc. Natl. Acad. Sci. U. S. A. 117 (2020) 12071–12079, https://doi.org/10.1073/pnas.2003475117.
[63] N.C. Schoendorfer, R. Obeid, L. Moxon-Lester, N. Sharp, L. Vitetta, R.N. Boyd, P. S. Davies, Methylation capacity in children with severe cerebral palsy, Eur. J. Clin. Investig. 42 (2012) 768–776, https://doi.org/10.1111/j.1365-2362.2011.02644.x.
[64] J. Sanderson, D.A. Dartt, V. Trinkaus-Randall, J. Pintor, M.M. Civan, N. A. Delamere, E.L. Fletcher, T.E. Salt, A. Grosche, C.H. Mitchell, Purines in the eye: recent evidence for the physiological and pathological role of purines in the RPE, retinal neurons, astrocytes, Müller cells, lens, trabecular meshwork, cornea and lacrimal gland, Exp. Eye Res. 127 (2014) 270–279, https://doi.org/10.1016/j.exer.2014.08.009.
[65] A. Kumar, S. Giri, A. Kumar, 5-Aminoimidazole-4-carboxamide ribonucleoside-mediated adenosine monophosphate-activated protein kinase activation induces protective innate responses in bacterial endophthalmitis, Cell. Microbiol. 18 (2016) 1815–1830, https://doi.org/10.1111/cmi.12625.
[66] C. Jang, S. Hui, X. Zeng, A.J. Cowan, L. Wang, L. Chen, R.J. Morscher, J. Reyes, C. Frezza, H.Y. Hwang, A. Imai, Y. Saito, K. Okamoto, C. Vaspoli, L. Kasprenski, G. A. Zsido 2nd, J.H. Gorman 3rd, R.C. Gorman, J.D. Rabinowitz, Metabolite exchange between mammalian organs quantified in pigs, Cell Metab. 30 (2019) 594–606, e3, https://doi.org/10.1016/j.cmet.2019.06.002.
[67] M. Giarmarco, M. Kanow, A. Engel, J. Du, J.R. Chao, J. Hurley, Fuel exchange between photoreceptors and RPE underlies a retinal metabolic ecosystem, Invest. Ophthalmol. Vis. Sci. 58 (2017) 3018.
[68] O. Strauss, The retinal pigment epithelium in visual function, Physiol. Rev. 85 (2005) 845–881, https://doi.org/10.1152/physrev.00021.2004.
[69] J.D. Weisfeld-Adams, E.A. McCourt, G.A. Diaz, S.C. Oliver, Ocular disease in the cobalamin C defect: a review of the literature and a suggested framework for clinical surveillance, Mol. Genet. Metab. 114 (2015) 537–546, https://doi.org/10.1016/j.ymgme.2015.01.012.
[70] G.J. Chader, Animal models in research on retinal degenerations: past progress and future hope, Vis. Res. 42 (2002) 393–399, https://doi.org/10.1016/s0042-6989(01)00212-7.
[71] L.D. Carter-Dawson, M.M. LaVail, Rods and cones in the mouse retina. I. Structural analysis using light and electron microscopy, J. Comp. Neurol. 188 (1979) 245–262, https://doi.org/10.1002/cne.901880204.
[72] T.D. Lamb, Why rods and cones? Eye 30 (2015) 179–185, https://doi.org/10.1038/eye.2015.236.
[73] G.T. Prusky, R.M. Douglas, Characterization of mouse cortical spatial vision, Vis. Res. 44 (2004) 3411–3418, https://doi.org/10.1016/j.visres.2004.09.001.
[74] M. Fruttiger, Development of the mouse retinal vasculature: angiogenesis versus vasculogenesis, Invest. Ophthalmol. Vis. Sci. 43 (2002) 522–527.
[75] M. Fruttiger, Development of the retinal vasculature, Angiogenesis 10 (2007) 77–88, https://doi.org/10.1007/s10456-007-9065-1.
[76] A.D. Huberman, C.M. Niell, What can mice tell us about how vision works? Trends Neurosci. 34 (2011) 464–473, https://doi.org/10.1016/j.tins.2011.07.002.
[77] C.-J. Jeon, E. Strettoi, R.H. Masland, The major cell populations of the mouse retina, J. Neurosci. 18 (1998) 8936–8946, https://doi.org/10.1523/jneurosci.18-21-08936.1998.